
Deep Exploration with PAC-Bayes

Bahareh Tasdighi¹ Manuel Haussmann¹ Nicklas Werge¹ Yi-Shan Wu¹ Melih Kandemir¹

Abstract

Reinforcement learning for continuous control under delayed rewards is an under-explored problem despite its significance in real life. Many complex skills build on intermediate ones as prerequisites. For instance, a humanoid locomotor has to learn how to stand before it can learn to walk. To cope with delayed reward, a reinforcement learning agent has to perform deep exploration. However, existing deep exploration methods are designed for small discrete action spaces, and their successful generalization to state-of-the-art continuous control remains unproven. We address the deep exploration problem for the first time from a PAC-Bayesian perspective in the context of actor-critic learning. To do this, we quantify the error of the Bellman operator through a PAC-Bayes bound, where a bootstrapped ensemble of critic networks represents the posterior distribution, and their targets serve as a data-informed function-space prior. We derive an objective function from this bound and use it to train the critic ensemble. Each critic trains an individual soft actor network, implemented as a shared trunk and critic-specific heads. The agent performs deep exploration by acting epsilon-greedily on a randomly chosen actor head. Our proposed algorithm, named *PAC-Bayesian Actor-Critic (PBAC)*, is the only algorithm to consistently discover delayed rewards on a diverse set of continuous control tasks with varying difficulty.

and collecting keys in the correct order. An intelligent agent has to identify and solve these sub-tasks based solely on the final reward. Deep reinforcement learning (RL) has proven effective at these sparse reward scenarios, with AlphaZero (Silver et al., 2018) and Random Network Distillation (Burda et al., 2019) reaching superhuman performance in chess and Montezuma’s Revenge, respectively, despite receiving zero reward for long interaction sequences.

Continuous control tasks share a similar modular structure. There is strong evidence that biological systems execute complex movements through robust and stable building blocks, known as motion primitives (Flash & Hochner, 2005). Application of the same idea to robotics, dynamic movement primitives (Schaal, 2006), demonstrated remarkable success when unit movement patterns are fit to observations separately and an agent is trained to apply them in a sequence. This works well when the target environment is well-understood and eligible for a rigorous engineering effort. However, performing loosely defined tasks in open-world scenarios requires approaches that both invent these primitives from authentic environment interactions and use them in an optimal order for task completion within feasible sample complexity limits. Reinforcement learning has not yet delivered success stories in continuous control setups with delayed rewards. Here we use the term *delayed rewards* to refer both to settings where no reward is received until a task is solved, i.e., sparse ones, and to those where constant negative reward is received until a task is solved.

Reinforcement learning for delayed rewards commonly focuses on quantifying Bellman target uncertainty for exploration. The scheme, *deep exploration* (Osband et al., 2016a), should aim for multi-step information gains by propagating uncertainty across Bellman backups. Several model-free approaches treat this as a Bayesian inference problem on the Bellman target (Osband et al., 2016a; 2018; Touati et al., 2020; Fellows et al., 2024). Model-based approaches explore by propagating the uncertainty of a learned state transition kernel through the value function to estimate the Bellman target uncertainty (O’Donoghue et al., 2018; Luis et al., 2023a). Finally, pseudo-count-based approaches occupy a middle-ground between these and aim to estimate the visitation count of state-action pairs by distilling a randomly initialized predictor into a parametric auxiliary network (Nikulin et al., 2023; Yang et al., 2024; Burda et al., 2019).

1. Introduction

Complex control tasks commonly require completing sequential sub-tasks. For example, in chess this means executing theoretically correct opening moves, creative and tactical mid-game combinations, and a precise endgame. Similarly, Montezuma’s Revenge requires navigating rooms

¹Department of Mathematics and Computer Science University of Southern Denmark. Correspondence to: Bahareh Tasdighi <tasdighi@imada.sdu.dk>.

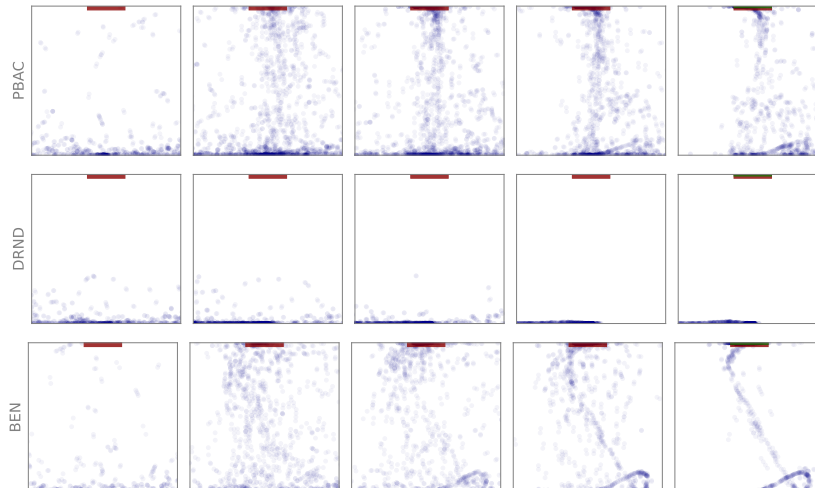


Figure 1. *Deep exploration.* State exploration patterns of state and angle dimensions in the cartpole environment are visualized as training progresses (random trajectories are displayed throughout the training phase). DRND (Yang et al., 2024) fails able to explore enough. Both BEN (Fellows et al., 2024) and PBAC (ours) are quickly able to identify the target region (red box). While BEN switches to full exploitation, our model is able to achieve the same performance (see Table 1), while continuing to remain flexible enough to explore.

A few recent model-based approaches (Luis et al., 2023a) show success in continuous control tasks at the expense of a prohibitive computational overhead for model learning and a strong dependency on learnable environment dynamics.

Contribution. We formulate the deep exploration problem from a Probably Approximately Correct (PAC) Bayesian (McAllester, 1999; Alquier, 2024) perspective and present an actor-critic algorithm that reaches unprecedented performance in continuous control with delayed rewards. We quantify the Bellman operator error using a Catoni-type PAC-Bayes bound (Catoni, 2007) for the first time in a policy evaluation context. We use a bootstrapped ensemble of critic networks as an empirical posterior distribution and build a data-informed function-space prior from their target networks. To train this ensemble, we derive a simple and intuitive objective function. As the actor, we use a probabilistic network with a shared trunk and multiple heads, each assigned to a separate critic. We apply posterior sampling during training for exploration and Bayesian model averaging during evaluation. We conduct experiments on a diverse set of continuous control tasks, both established and novel, some of which have reward structures significantly more challenging than the prior art. Our *PAC-Bayesian Actor-Critic (PBAC)* algorithm is the only model capable of solving these tasks, whereas both state-of-the-art and well-established methods fail in several. Figure 1 visualizes PBAC’s deep exploration followed by effective exploitation, while remaining flexible enough to explore the state space and to adapt to potential new reward regions.

2. Background and prior art

2.1. Reinforcement learning

Consider a measurable space $(\mathcal{S}, \sigma(\mathcal{S}))$ of a set of states \mathcal{S} an agent may be in and its corresponding σ -algebra $\sigma(\mathcal{S})$ comprising all measurable subsets of \mathcal{S} and an action space \mathcal{A} from which an agent chooses an action to interact with its environment. We define a Markov Decision Process (MDP) (Puterman, 2014) as a tuple $M = \langle \mathcal{S}, \mathcal{A}, r, P, P_0, \gamma \rangle$, where $r : \mathcal{S} \times \mathcal{A} \rightarrow [0, R]$ is a bounded reward function, $P : \mathcal{S} \times \mathcal{A} \times \sigma(\mathcal{S}) \rightarrow [0, 1]$ is a state transition kernel giving the probability of the next state $s' \in \mathcal{S}$ for the current state-action pair (s, a) , $P_0 : \sigma(\mathcal{S}) \rightarrow [0, 1]$ is an initial state distribution, and $\gamma \in [0, 1)$ is a discount factor. For a policy $\pi : \mathcal{S} \rightarrow \mathcal{A}$, RL aims to maximize the expected sum of discounted rewards

$$\pi^* \in \arg \max_{\pi \in \Pi} \mathbb{E}_{\tau_\pi} \left[\sum_{t=0}^{\infty} \gamma^t r(s_t) \right],$$

where the expectation is taken with respect to a trajectory $\tau_\pi := (s_0, a_0, s_1, a_1, s_2, a_2, \dots)$ of states and actions that occur when a policy π chosen from a feasible set Π is employed. The exact Bellman operator for a policy π is

$$T_\pi Q(s, a) = r(s, a) + \gamma \mathbb{E}_{s' \sim P(\cdot | s, a)} [Q(s', \pi(s'))],$$

where $Q : \mathcal{S} \times \mathcal{A} \rightarrow \mathbb{R}$. The unique fixed point of this operator is the true action-value function Q_π that maps a state-action pair (s, a) to the discounted reward π collects when executed starting from (s, a) , that is $T_\pi Q(s, a) = Q(s, a)$ if and only if $Q(s, a) = Q_\pi(s, a), \forall (s, a)$. Any other Q incurs an error $T_\pi Q(s, a) - Q(s, a) > 0$ for some (s, a) referred

to as the *Bellman error*. Define the squared P_π -weighted L_2 -norm as $\|f\|_{P_\pi}^2 = \int_{s \in \mathcal{S}} |f(s)|^2 dP_\pi(s)$ for some $f : \mathcal{S} \rightarrow \mathbb{R}$. We approximate the true action-value function Q_π by one-step Temporal Difference (TD) learning minimizing

$$L(Q) := \|T_\pi Q - Q\|_{P_\pi}^2 \quad (1)$$

with respect to Q given a data set \mathcal{D} . As the transition kernel is usually not known, a stochastic version of this loss has to be calculated via Monte Carlo samples

$$\tilde{L}(Q) := \mathbb{E}_{s \sim P_\pi} \left[\mathbb{E}_{s' \sim P(\cdot | s, \pi(s))} \left[(\tilde{T}_\pi Q(s, \pi(s), s') - Q(s, a))^2 \right] \right],$$

with the *sample Bellman operator*, defined as

$$\tilde{T}_\pi Q(s, a, s') = r(s, a) + \gamma Q(s', \pi(s')).$$

A deep RL algorithm fits an approximator Q to a set of observed tuples (s, a, s') stored in a replay buffer \mathcal{D} by minimizing an empirical estimate of the stochastic loss:

$$\hat{L}_{\mathcal{D}}(Q) := \frac{1}{|\mathcal{D}|} \sum_{(s, a, s') \in \mathcal{D}} \left(\tilde{T}_\pi Q(s, a, s') - Q(s, a) \right)^2.$$

The approximated Q function is used as a training objective in a subsequent policy optimization step. Temporal difference learning identifies the globally optimal policy when used for discrete MDPs. In the continuous case, it finds a local optimum (Bertsekas & Tsitsiklis, 1996) and quite often in a sample-inefficient way in real-world applications.

2.2. Deep exploration

The classical optimal control paradigm prescribes a rigorous design of cost functions, i.e., negative rewards, that give a dense signal about model performance at each stage of model fitting (Stengel, 1994; Kirk, 2004). This approach is akin to detailed loss designs, a common practice of deep learning. However, next-generation AI problems demand agents with high cognitive capabilities that autonomously learn smart strategies to reach distant high rewards without being trapped by intermediate small rewards or prematurely give up searching. These approaches do *deep exploration* (Osband et al., 2016a). They perform case-specific exploration based on their actual knowledge about the environment. Their common ground is to estimate how often a state-action pair has been visited until a certain training step and direct the exploration towards unvisited ones. Deep exploration approaches can be classified into four categories based on how accurate knowledge of environment dynamics they assume to make this estimation:

(i) *Model-based approaches* learn to infer the state transition kernel by a function approximator $P_\phi(\cdot | s, a) \approx P(\cdot | s, a)$

and use its uncertainty to generate *intrinsic rewards* (Chentanez et al., 2004) to perform curiosity-driven exploration, which has remarkable roots to biological intelligence (Schmidhuber, 2010; Modirshanechi et al., 2023). VIME (Houthoofd et al., 2016) incentivizes exploration of states that bring more information gain on the estimated kernel, while BYOL-Explore (Guo et al., 2022) and BYOL-Hindsight (Jarrett et al., 2023) choose states with higher prediction error. Approaches such as UBE (O’Donoghue et al., 2018), Exact UBE (Luis et al., 2023a), and QU-SAC (Luis et al., 2023b) choose the target quantity as the sample Bellman operator $\tilde{T}_\pi Q$. MOBILE (Sun et al., 2023) and MOPO (Yu et al., 2020b) are their offline RL counterparts.

(ii) *Pseudo-count approaches* learn to predict the relative visitation frequencies of state-action pairs without needing to predict state transitions. These frequencies are then used to generate intrinsic rewards directing the exploration towards less frequent state-action pairs. The commonplace approach, called *Random Network Distillation (RND)* (Burda et al., 2019), distills a fixed network with randomly initialized weights into another one with learned parameters. The distillation serves as a pseudo-count to generate intrinsic rewards. State-of-the-art variants include SAC-RND (Nikulin et al., 2023) and SAC-DRND (Yang et al., 2024).

(iii) *Randomized value iteration approaches* learn to estimate the uncertainty around the approximate Q function by modeling it as a random variable and performing posterior inference based on the observed Bellman errors. Proposed inference methods include Bayesian linear regression (Osband et al., 2016b), mean-field (Lipton et al., 2018) or structured (Touati et al., 2020) variational inference on Bayesian neural networks, Bayesian deep bootstrap ensembles with flat priors (Osband et al., 2016a) and informative priors (Osband et al., 2018). Fellows et al. (2021) show that these approaches infer a posterior on the Bellman target $T_\pi Q$ instead of the intended Q and propose to overcome the consequences of this mismatch by training a separate Q network on the posterior predictive mean of $T_\pi Q$. *Bayesian Exploration Networks (BEN)* (Fellows et al., 2024), a more advanced version of this approach, fits a Bayesian heteroscedastic neural net on the Bellman target using structured variational inference.

(iv) *Policy randomization approaches* propose different perturbations on the learned models to randomize the employed policy without aiming to quantify the uncertainty of a quantity. Proposed solutions include perturbing the Q -network weights for discrete action spaces (Fortunato et al., 2018), actor-network weights (Plappert et al., 2018) for continuous control, and transforming the policy distribution by normalizing flows (Mazouze et al., 2019).

In this work, we follow the randomized value iteration approach due to its balance between computational feasibility

and theoretical soundness. Bayesian model averaging gives the optimal decision rule for an approximate Q function with partial observation on an MDP with reliable uncertainty estimates (Cox & Hinkley, 1974). The use of PAC-Bayes in reinforcement learning is limited to theoretical analysis (Fard et al., 2012) and preliminary developments aiming to improve training robustness (Tasdighi et al., 2024).

2.3. PAC-Bayesian analysis and learning

Given input \mathcal{Z} , output \mathcal{Y} , and hypothesis spaces $\mathcal{H} = \{h : \mathcal{Z} \rightarrow \mathcal{Y}\}$, and loss function $\ell : \mathcal{Y} \times \mathcal{Y} \rightarrow [0, B]$, we define the empirical risk \widehat{L} on observations $\mathcal{O} = \{(z_i, y_i) : (z_i, y_i) \sim P_D, i \in [n]\}^1$ containing n samples from a distribution P_D , and the true risk L as

$$\widehat{L}_{\mathcal{O}}(h) = \frac{1}{n} \sum_{i=1}^n \ell(h(z_i), y_i),$$

$$L(h) = \mathbb{E}_{(z,y) \sim P_D} [\ell(h(z), y)].$$

PAC-Bayesian analysis (Shawe-Taylor & Williamson, 1997; Alquier, 2024) provides an upper bound C of the form $d(\mathbb{E}_{h \sim \rho} [L(h)], \mathbb{E}_{h \sim \rho} [\widehat{L}_{\mathcal{O}}(h)]) \leq C(\rho, \rho_0, \delta)$ that holds with probability at least $1 - \delta$ for any error tolerance $\delta \in (0, 1]$ and any prior probability measure ρ_0 and posterior probability measure ρ chosen from the set of all measures \mathcal{P} feasible on the hypothesis space \mathcal{H} for a given convex distance metric $d(\cdot, \cdot)$. The choice of the posterior measure ρ can depend on the data \mathcal{O} while the prior measure ρ_0 cannot, hence their names. Unlike in Bayesian inference, the posterior and the prior do not need to relate to each other via a likelihood function. The prior serves as a reference with respect to which a generalization statement is made. Of the various well-known PAC-Bayes bounds (such as McAllester (1999); Seeger (2002); Germain et al. (2009)) we build on Catoni (2007)’ bound in this work.

Theorem 1 (Catoni (2007)). *For distributions ρ, ρ_0 measurable on hypothesis space \mathcal{H} , $\nu > 0$, and error tolerance $\delta \in (0, 1)$, the following inequality holds with probability greater than $1 - \delta$.*

$$\mathbb{E}_{h \sim \rho} [L(h)] \leq \mathbb{E}_{\rho} [\widehat{L}(h)] + \frac{\nu C^2}{8n} + \frac{\text{KL}(\rho \parallel \rho_0) - \log \delta}{nu},$$

where C is the upper bound on L .

Here, $\text{KL}(\rho \parallel \rho_0) = \mathbb{E}_{h \sim \rho} [\log \rho(h) - \log \rho_0(h)]$ is the Kullback-Leibler divergence between ρ and ρ_0 .

Since a PAC-Bayes bound holds for any posterior, a parametric family of posteriors can be chosen and its parameters can be fit to data by minimizing the right-hand side of the bound. This approach, called *PAC-Bayesian Learning*, demonstrated remarkable success in image classification

(Dziugaite & Roy, 2017; Wu et al., 2024) and regression (Reeb et al., 2018). There exist only preliminary results such as Tasdighi et al. (2024) that use this approach in deep reinforcement learning. The tightness of the bound is determined by the choice of d , as well as additional assumptions and algebraic manipulations on the second term on the right-hand side of the inequality. Remarkably, this term does not depend on ρ , and hence does not play any role in a PAC-Bayesian learning algorithm. Our solution relies on this simple but often overlooked observation.

3. Deep exploration via PAC-Bayes

3.1. Theory

We build an actor-critic algorithm able to perform deep exploration in continuous control setups with delayed rewards and consider a model-free and off-policy approximate temporal difference training setup. The only existing prior work at the time of writing that addresses this setup with a PAC-Bayesian analysis is by Fard et al. (2012). This work uses PAC-Bayes to directly bound the value of a policy from a single chain of observations. The Markovian dependencies of these observations necessitate building on a Bernstein-like concentration inequality that only works for extremely long episodes, prohibiting its applicability to PAC-Bayesian learning (Tasdighi et al., 2024). We overcome this limitation by instead developing a PAC-Bayes bound on the Bellman operator error. See Appendix A for proofs on all results.

We assume the existence of a replay buffer \mathcal{D} containing samples obtained from real environment interactions. Following Fard et al. (2012), we assume for convenience that the policy π being evaluated always induces a stationary state transition kernel, that is $P_{\pi}(s') = \int P(s'|s, \pi(s))P_{\pi}(s)ds$ for every $s \in \mathcal{S}$ in all training-time environment interactions, where P_{π} denotes the state visitation distribution for policy π . This is essentially a hidden assumption made by the commonplace off-policy deep reinforcement learning algorithms that take uniformly random batches from their replay buffers. The difference between the sample Bellman operator and the Bellman operator, $\widetilde{T}_{\pi}Q(s, a, s') - T_{\pi}Q(s, \pi(s))$, is known to tend to an accumulating positive value when Q is concurrently used as a training objective for policy improvement, leading to a phenomenon known as *overestimation bias* (Thrun & Schwartz, 1993). The problem is tackled by approaches such as double Q -learning (Van Hasselt, 2010) and min-clipping (Fujimoto et al., 2018). We define with

$$X(s, a) \stackrel{d}{=} Q(s, a) + \widetilde{T}_{\pi}Q(s, a, s') - T_{\pi}Q(s, a),$$

for all $(s, a) \sim \mathcal{S} \times A$, a new random variable, where $\stackrel{d}{=}$ denotes equality in distribution. This is a hypothetical variable that predicts from (s, a) the value of the observed Bellman

¹Throughout $[m]$ denotes the set $\{1, \dots, m\}$ for $m \in \mathbb{N}$.

target caused by the randomness of s' . It is related to the action-value function approximator as

$$\begin{aligned} Q(s, a) &= \\ & Q(s, a) + \mathbb{E}_{s' \sim P(\cdot | s, a)} \left[\tilde{T}_\pi Q(s, a, s') \right] - T_\pi Q(s, a) \\ &= \mathbb{E}_{s' \sim P(\cdot | s, a)} \left[Q(s, a) + \tilde{T}_\pi Q(s, a, s') - T_\pi Q(s, a) \right] \\ &= \mathbb{E}[X(s, a)]. \end{aligned}$$

Let ρ denote the distribution of X , then the one-step TD loss can be expressed as

$$\begin{aligned} L(Q) &= \|T_\pi Q - Q\|_{P_\pi}^2 = \|T_\pi Q - \mathbb{E}[X]\|_{P_\pi}^2 \\ &= \mathbb{E}_{s \sim P_\pi} \left[\left(\mathbb{E}_{s' \sim P(\cdot | s, \pi(s))} [r(s, \pi(s)) \right. \right. \\ &\quad \left. \left. + \gamma \mathbb{E}[X(s', \pi(s'))] \right] - \mathbb{E}[X(s, \pi(s))] \right)^2 \right], \end{aligned}$$

with the corresponding stochastic variant²

$$\begin{aligned} \tilde{L}(\rho) &= \mathbb{E}_{s \sim P_\pi} \mathbb{E}_{s' \sim P(\cdot | s, \pi(s))} \left[\right. \\ &\quad \left. \mathbb{E}_{X \sim \rho} \left[\left(\tilde{T}_\pi X(s, \pi(s), s') - X(s, \pi(s)) \right)^2 \right] \right]. \end{aligned}$$

This optimization problem no longer fits a deterministic map Q but instead infers a distribution ρ that best describes the action-value function perturbed by the Bellman operator error. The loss can be interpreted as the true risk of a Gibbs predictor $X \sim \rho$. The corresponding empirical risk is

$$\begin{aligned} \hat{L}_{\mathcal{D}}(\rho) &= \\ & |D|^{-1} \sum_{(s, a, s') \in \mathcal{D}} \mathbb{E}_{X \sim \rho} \left[\left(\tilde{T}_\pi X(s, a, s') - X(s, \pi(s)) \right)^2 \right]. \end{aligned}$$

We formulate our learning problem as selecting ρ from a feasible set \mathcal{P} to achieve the tightest PAC-Bayes bound on $\tilde{L}(\rho)$ with respect to data \mathcal{D} and a prior $\rho_0 \in \mathcal{P}$ over the distribution of X . This bound gives generalization guarantees on how well X can predict a noisy Bellman operator output. However, our main goal is to minimize the value estimation error $\|Q_\pi - Q\|_{P_\pi} = \|Q_\pi - \mathbb{E}[X]\|_{P_\pi}$, upper bounded via Jensen's inequality by $\mathbb{E}_{X \sim \rho} \|Q_\pi - X\|_{P_\pi}$. Prior work (Fellows et al., 2021) addresses the mismatch between target and inferred quantities in probabilistic reinforcement learning and its consequences. We propose an alternative solution by leveraging on the contraction property of Bellman operators and the following result.

Lemma 1. *For any ρ defined on X , we have*

$$\begin{aligned} \tilde{L}(\rho) &= \mathbb{E}_{X \sim \rho} \|T_\pi X - X\|_{P_\pi}^2 \\ &\quad + \gamma^2 \mathbb{E}_{X \sim \rho} [\text{Var}_{s \sim P_\pi} [X(s, \pi(s))]]. \end{aligned}$$

²A realization of X shares the same domain and range as Q . Hence it can be passed through the sample Bellman operator \tilde{T} .

Applying the contraction property of Bellman operators to $\|T_\pi X - X\|_{P_\pi}^2$ (see Lemma 2) and adding all quantities into Theorem 1's generic bound, we arrive at our main result.

Theorem 2. *For any posterior and prior measures $\rho, \rho_0 \in \mathcal{P}$, error tolerance $\delta \in (0, 1]$, and policy π , simultaneously, the following inequality holds with probability at least $1 - \delta$:*

$$\begin{aligned} \mathbb{E}_{X \sim \rho} \|Q_\pi - X\|_{P_\pi}^2 &\leq \left(\hat{L}_{\mathcal{D}}(\rho) \right. \\ &\quad \left. + \frac{\nu \bar{\lambda} B^2}{8n} + \frac{\text{KL}(\rho \| \rho_0) - \log \delta}{\nu} \right. \\ &\quad \left. - \gamma^2 \mathbb{E}_{X \sim \rho} \text{Var}_{s \sim P_\pi} [X(s, \pi(s))] \right) / (1 - \gamma)^2, \end{aligned} \quad (2)$$

where $\bar{\lambda} \triangleq \frac{1 + \max_{t \in [n]} \lambda_t}{1 - \max_{t \in [n]} \lambda_t}$ with $\lambda_t \in [0, 1]$ as the operator norm of the transition kernel of the time-inhomogeneous Bellman error Markov chain at time t , $B = R^2 / (1 - \gamma)^2$ and $\nu > 0$ an arbitrary constant.

Note that $\max_{t \in [n]} \lambda_t \rightarrow 1$ would imply a chain with an absolute correlation with the past. As $\bar{\lambda}$ and B independent of the posterior, we ignore it in the subsequent derivation of the training objective. Our main concern is to develop an algorithm using learning-theoretic tools and not to provide tight performance guarantees. Tighter guarantees can be given by plugging the learned posterior into an existing bound rigorously developed for a specific purpose. We discuss $\bar{\lambda}$ and B in greater detail in Appendix A and derive an alternative bound by following Fard et al. (2012).

3.2. Implementation

To design a learning algorithm from the bound, we require several approximations.³

(i) Model the posterior ρ with an ensemble. To have a flexible and powerful posterior distribution, we learn an ensemble of K critics $\{X_k : \mathcal{S} \times \mathcal{A} \rightarrow \mathbb{R} \mid k \in [K]\}$ parameterized by weights θ_k , and model $\rho(A) := \frac{1}{K} \sum_{k=1}^K \delta_{X_k}(A)$, for $A \in \sigma(\mathcal{S})$ and Dirac measure δ . We extend this with a set of target copies, \bar{X}_k , updated by Polyak averaging, $\bar{\theta}_k \leftarrow (1 - \tau)\bar{\theta}_k + \tau\theta_k$, for $\tau \in [0, 1]$. For a single observation, the empirical risk term is $\frac{1}{K} \sum_{k=1}^K (r + \gamma \bar{X}_k(s', \pi(s')) - X_k(s, a))^2$ where we use \bar{X}_k to ensure robust training (Lillicrap et al., 2016).

(ii) Model the distributions in function-space instead of weight-space. Deep reinforcement learning setups use action-value functions in downstream tasks during training, e.g., exploration, bootstrapping, and actor training. Design choices such as how much to explore and how conservatively to evaluate the Bellman target can only be made on the function space. Furthermore, according to the data processing inequality (Polyanskiy & Wu, 2014, Theorem 6.2), the

³See Appendix C for a pseudocode summary.

function-space view yields a tighter generalization bound than the weight-space view. The KL divergence between two measures ρ, ρ_0 defined on \mathcal{H} is via Rudner et al. (2022):

$$\text{KL}(\rho \parallel \rho_0) = \sup_{\mathcal{D} \in \mathcal{B}} \mathbb{E}_{s \in \mathcal{D}} [\mathbb{E}_{X \sim \rho} [\log f_\rho(X|s, \pi(s)) - \log f_{\rho_0}(X|s, \pi(s))]],$$

where f_ρ and f_{ρ_0} are the probability density functions of the two measures evaluated at X for a given state-action pair and \mathcal{B} is the space of all possible data sets \mathcal{D} . As the sup calculation is intractable in practice. We simplify Rudner et al. (2022)’s approximation of the supremum to

$$\sum_{j=1}^J \sum_{i=1}^{|B_j|} \log f_\rho(s_i, \pi(s_i)) - \log f_{\rho_0}(s_i, \pi(s_i)) \quad (3)$$

where B_j are minibatches sampled from the available data set. This is valid as the sum of a set of scalars upper bounds their supremum. We are not aware of any earlier application of function-space priors in the context of PAC-Bayesian learning, especially related to reinforcement learning.

(iii) Introduce a data-dependent prior ρ_0 . Inspired by prior work on PAC Bayes outside the reinforcement learning context (Ambroladze et al., 2006; Dziugaite & Roy, 2018), we adopt a data-informed prior ρ_0 to attain a tight PAC Bayes bound that can be used more reliably for policy evaluation. As the most recent and robust information about the action values are stored in the targets \bar{X}_k , we use them to build a maximum likelihood estimate of a normal density. The target networks are trained to evaluate the next state action-values and we choose $f_{\rho_0}(s', \pi(s')) = \mathcal{N}(\bar{\mu}_\pi(s'), \sigma_0^2)$ where $\bar{\mu}_\pi(s') = \frac{1}{K} \sum_{k=1}^K \bar{X}_k(s', \pi(s'))$. Projecting this random variable one-time step backwards, we get $f_{\rho_0}(s, \pi(s)) := \mathcal{N}(r + \gamma \bar{\mu}_\pi(s'), \gamma^2 \sigma_0^2)$ where r is the reward observation related to state s . Note that the use of critic targets does not violate the PAC-Bayes bound as ρ_0 is built on critic targets evaluated at the previous gradient step while the bound is given only for the current minibatch.

(iv) Approximate equation (3) analytically. The posterior ρ defined in Step (i) does not have an analytical density function. We approximate its appearance in the KL divergence by a normal density $f_\rho(s, \pi(s)) := \mathcal{N}(\mu_\pi(s), \sigma_\pi^2(s))$ where μ is calculated as in Step (iii) but on the learned critic networks X_i instead of their targets and $\sigma_\pi^2(s) = \frac{1}{K-1} \sum_{k=1}^K (X_k(s, \pi(s)) - \mu_\pi(s))^2$ on the current state s instead of the next one. Although $\text{KL}(f_\rho \parallel f_{\rho_0})$ now has an analytical solution, we approximate it as

$$\begin{aligned} & \text{KL}(\rho(s, \pi(s)) \parallel \rho_0(s, \pi(s))) \\ & \approx \frac{1}{2K} \sum_{k=1}^K \left(\frac{(r + \gamma \bar{\mu}_\pi(s') - X_k)^2}{\gamma^2 \sigma_0^2} - \log \sigma_\pi^2(s) \right) + \text{const}, \end{aligned}$$

to ensure that the computation stays closer to the true posterior. See Appendix A for the full details of the derivation.

(v) Decrease the influence of the variance in (2). Since $\log(x) < x, \forall x \in \mathbb{R}^+$, taking the logarithm of the expected variance term in (2) increases the inequality, while keeping it valid. We use this version to ensure that the impact of increased ensemble element variances on the loss diminishes gradually. Although the former option also learns, this version tends to improve the performance even further.

(vi) Apply bootstrapping. We apply bootstrapping to detach the correlation between the ensemble elements, which has significant practical benefits demonstrated in prior work on deep exploration (Osband et al., 2016a; 2018). We pass each minibatch through a random binary mask which filters some portion of the data for each ensemble element.

Combining these steps, our critic training objective becomes

$$\begin{aligned} L(\{X_k : k \in [K]\}) := & \\ & \underbrace{\frac{1}{nK} \sum_{i=1}^n \sum_{k=1}^K b_{ik} (r_i + \gamma \bar{X}_k(s'_i, \pi(s'_i)) - X_k(s_i, \pi(s_i)))^2}_{\text{Diversity}} \\ & + \underbrace{\frac{1}{nK} \sum_{i=1}^n \sum_{k=1}^K \frac{b_{ik} (r_i + \gamma \bar{\mu}_\pi(s'_i) - X_k(s_i, \pi(s_i)))^2}{2\gamma^2 \sigma_0^2}}_{\text{Coherence}} \\ & - \underbrace{\frac{2\gamma^2 + 1}{2n} \sum_{i=1}^n \log \sigma_\pi^2(s_i)}_{\text{Propagation}} \quad (4) \end{aligned}$$

for binary bootstrap masks $b_{ik} \sim \text{Bernoulli}(1 - \kappa)$, $\forall [n] \times [K]$ with a bootstrapping rate $\kappa \in (0, 1)$.⁴ The loss is computed by one forward pass through each ensemble member (run in parallel) and their targets per data point with additional constant-time operations. Hence its computation time is similar to any other actor-critic method. The loss contains three terms with interpretable roles. The first induces *diversity* into the ensemble by training each member on individual targets. This way the model quantifies the uncertainty of its predictions as observations assigned to similar action values that can only be those all ensemble elements are familiar with. The second term ensures *coherence* among ensemble elements as it trains them with the same target. The third term is a regularizer that repels ensemble elements away from each other in the absence of counter-evidence. This way, uncertainty *propagation* is maintained, as the model cannot find a solution to collapse the ensemble elements into a single solution. Propagation of uncertainties across time steps is known to have a critical role in deep exploration

⁴We calculate $\bar{\mu}_\pi$ and σ_π^2 after applying the bootstrap masks.

(Osband et al., 2018). As the variance increases, the PBAC loss converges to BootDQN-P (Osband et al., 2018). As it shrinks, it converges to the deterministic policy gradient.

The PBAC critic training loss nicely unifies the advantages of variational Bayesian inference (Blei et al., 2017) and Bayesian deep ensembles (Lakshminarayanan et al., 2017) into a single theoretically backed framework. Unlike variational Bayes, it works for density-free posteriors and unlike Bayesian deep ensembles, it permits a justified use of prior regularization via the Kullback-Leibler divergence term.

Actor training and behavior policy. We use an actor network with a shared trunk $g(s)$ and individual heads $\pi_k(s) := (h_k \circ g)(s)$ for each ensemble element. Since the optimal decision rule under uncertainty is the Bayes predictor, we train the actor on the average value of each state with respect to the learned posterior $\arg \max_{\pi} \mathbb{E}_{s \sim P_{\pi}} \mathbb{E}_{X \sim \rho} X(s, \pi(s))$ and implement its empirical approximation as $\arg \max_{g, h_1, \dots, h_K} \frac{1}{nK} \sum_{i=1}^n \sum_{k=1}^K X_k(s, \pi_k(s))$. We perform posterior sampling for exploration counting on its demonstrated theoretical benefits (Strens, 2000; Osband et al., 2013; Grande et al., 2014) and practical success in discrete control (Osband et al., 2016a; 2018; Fellows et al., 2021). That is, our behavior policy is randomly chosen among the available K options and fixed for a number of time steps as practiced in prior work (Touati et al., 2020). In critic training, the Bellman targets are computed with the active behavior policy. See Appendix C and B.4 for further algorithmic details and our hyperparameter choices.

4. Experiments

With the experimental evaluation, we validate our theoretical claims on improved performance on challenging deep exploration tasks with sparse and delayed rewards. Focusing on environments with nonlinear dynamics and continuous state and action spaces, we rely on a mixture of established sparse benchmarks from the DMC suite (Tassa et al., 2018), robotic tasks from Meta-World environments with sparse reward (Yu et al., 2020a), and introduce new delayed reward benchmarks based on various MuJoCo environments (Todorov et al., 2012). We evaluate whether PBAC improves performance in these setups with difficult reward characteristics while remaining competitive on their original standard dense reward counterparts. In Appendix B.1 we discuss prior work on such environments.

We build an ensemble of ten Q-functions and use a replay ratio of five to improve sample efficiency. This approach has been shown to achieve the same level of performance as state-of-the-art methods, effectively addressing sample efficiency, as shown by Nauman et al. (2024). More details on the reward structure of each environment and the remaining

design choices are provided in Appendix B. We provide a public implementation at `anonymous`.

Baselines. We compare our method with other state-of-the-art exploration approaches on three standard MuJoCo setups, their delayed versions along with three sparse DMC tasks, and seven Meta-World environments. We choose SAC-DRND (Yang et al., 2024) as the best representative of the RND family integrated to SAC, and BootDQN-P (Osband et al., 2018) as a close SOTA Bayesian model-free method to our model. Finally, BEN (Fellows et al., 2024) as the best representative approach that can learn the Bayes-optimal policies. See Appendix B for further details.

DMC. We report three sparse environments, ballincup, cartpole, and reacher, from the DMC suite in Table 1.

MuJoCo. To model reward sparsity in the MuJoCo environments, we explore the following two variations:

- (i) A *delayed* version in which the health reward is always set to zero which removes any incentive for the agent to maintain stability. This can cause the agent to prioritize speed (minimizing positional delay), potentially leading to inefficient movement patterns such as falling, rolling, or chaotic behavior. Without incentives for stability, the agent may fail to learn proper locomotion, resulting in suboptimal performance, harder training, and reduced overall effectiveness.
- (ii) A *very delayed* version in which the forward reward proportional to velocity is granted only if the agent reaches a distance threshold c . The degree of delay, which determines the task difficulty, increases proportionally to c . This delay is applied on top of the zero health reward from above. Although this incentivizes reaching the target, the lack of intermediate rewards for progress may lead the agent to struggle with exploration, resulting in slower learning and difficulty in discovering effective policies as the agent infrequently gains informative signals.

In these settings, the agent does not receive any positive reward and pays a penalty for using its actuators for failed explorations. Hence, they are well-suited for testing how directed the exploration scheme of a learning algorithm is. We use them to assess whether an exploration strategy can consistently promote effective exploration, when the agent encounters a lack of informative feedback during learning. Additionally, we report their dense counterparts.

We summarize our results in Table 1, reporting the interquartile mean (IQM) (Agarwal et al., 2021) together with the corresponding interquartile range over ten seeds. Reported are the reward on the final episode, and the area under learning curve (AULC) for the whole training period, which quantifies the convergence speed. See Figure 2 for the reward

Table 1. *DMC and MuJoCo*. InterQuartile Mean (IQM) scores over ten seeds with [lower, upper] quantiles. The three blocks report the DMC environment, and the dense and delayed MuJoCo environments. A higher IQM indicates better performance. For each task, we make the IQM values bold if they fall within the range of the highest IQM score.

ENVIRONMENT	(a) Final episode reward				(b) Area under learning curve			
	BEN	BootDQN-P	DRND	PBAC (ours)	BEN	BootDQN-P	DRND	PBAC (ours)
ballincup	977 [971,980]	973 [965,978]	973 [970,977]	979 [975,984]	954 [936,963]	801[778,861]	863[773,951]	828[815,923]
cartpole	796 [186,836]	601[379,770]	0.0[0.0,0.0]	778 [758,806]	423 [179,513]	527 [412,609]	0.0[0.0,0.0]	397[369,442]
reacher	903[799,975]	959 [911,965]	846[762,875]	942 [875,964]	708 [628,734]	730 [698,764]	624[494,695]	708 [677,792]
ant	5579[5114,5685]	298[114,430]	3337[2250,4363]	6428 [6287,6527]	3103[2719,3387]	511[486,547]	1799[596,2613]	4485 [4379,4848]
hopper	1051[567,1443]	1988 [1260,2494]	1864 [1103,2914]	1603 [1387,1937]	839[733,986]	974[949,1005]	952[736,1365]	1436 [1283,1623]
humanoid	1706[1402,1909]	311[243,372]	5144 [4743,5879]	2372[1552,2750]	1227[1118,1295]	258[240,265]	2677 [2416,3026]	1235[1181,1346]
ant (delayed)	4580[3369,4980]	-432[-542,-339]	10.0[8.3,12.7]	5341 [5030,5402]	2705[1804,3126]	-307[-319,-288]	-0.9[-3.8,1.6]	3794 [3516,4007]
ant (very delayed)	2051[-1,3661]	-169[-291,-136]	-2.8[-2.8,-2.4]	4513 [3753,5048]	875[-16,1494]	-16[-76,53]	-7.6[-9.0,-6.0]	2937 [2622,3290]
hopper (delayed)	813 [689,928]	1067 [659,1340]	440[295,525]	963 [761,1121]	611[554,734]	275[170,394]	309[267,368]	793 [704,1025]
hopper (very delayed)	190 [6,643]	388 [-0.1579]	82[-0.347]	582 [429,745]	367 [72,537]	62[-0.248]	55[-0.250]	382 [274,507]
humanoid (delayed)	6.0[5.9,6.1]	-3.3[-13.6,4.6]	5.9[5.8,5.9]	690 [202,1715]	0.6[0.2,1.2]	-0.9[-3.5,1.9]	4.9[4.9,5.0]	214 [107,592]

Table 2. *Sparse Meta-World*. Average success rate percentage over five seeds on sparse Meta-World environments with hidden goals. A higher indicates better performance.

ENVIRONMENT	(a) average of the final episode success rate			
	BEN	BootDQN-P	DRND	PBAC (ours)
window close	0.20±0.40	0.00±0.00	0.98 ±0.04	0.86±0.28
window open	0.00±0.00	0.04±0.08	0.80±0.40	0.86 ±0.28
drawer close	0.96±0.08	0.62±0.47	1.00 ±0.00	0.92±0.16
drawer open	0.00±0.00	0.00±0.00	1.00 ±0.00	0.90±0.15
reach	0.60±0.49	0.00±0.00	0.80±0.40	1.00 ±0.00
button press topdown	0.00±0.00	0.00±0.00	0.20±0.40	0.62 ±0.40
door open	0.00±0.00	0.00±0.00	0.60±0.49	0.88 ±0.15
(b) average of the area under success rate curve				
window close	0.18±0.38	0.06±0.23	0.92±0.26	0.93 ±0.21
window open	0.00±0.00	0.15±0.36	0.76±0.43	0.77 ±0.34
drawer close	0.94±0.18	0.61±0.48	0.97 ±0.15	0.89 ±0.23
drawer open	0.00±0.00	0.00±0.00	0.81 ±0.39	0.77 ±0.34
reach	0.56±0.49	0.00±0.00	0.78±0.42	0.94 ±0.24
button press topdown	0.00±0.00	0.00±0.00	0.19±0.39	0.63 ±0.42
door open	0.00±0.00	0.00±0.00	0.50±0.49	0.83 ±0.32

curves throughout training. PBAC is competitive in most environmental settings and excels especially in the learning speed (subtable (b)) in delayed environments. Interquartile means that are not statistically significant at a level $p < 0.05$ to the highest IQM in a paired t-test are marked bold. We provide further details on this in the appendix.

Sparse Meta-World. In each task, the RL agent receives a reward of one upon reaching the goal and zero for the remainder. The goal location remains hidden in all environments. We evaluated our proposed PBAC model on the random-goal MT benchmark, where the hidden goal position changes with each trajectory. Our results provided in Table 2 show that PBAC outperforms the other baselines, demonstrating its ability to generalize effectively across different goal positions. More detailed information is provided in Appendix B.2 We report the final average success rate and the area under the success rate curve. Methods that do not perform significantly worse ($p < 0.05$) are marked bold.

Exploration patterns. Figure 1 shows how PBAC explores

the first two dimensions of the state space (position and angle) in the cartpole environment, throughout its training process. We describe this visualization in greater detail and include the remaining methods as well as a second environment (delayed ant) in Appendix D.2.

Hyperparameters. We provide results on the influence of the three main hyperparameters, bootstrap rate κ , posterior sampling rate, and prior variance σ_0 in Appendix B.4.

5. Conclusion

We introduced a method to do deep exploration in delayed reward environmental settings for the first time with a principled PAC-Bayesian approach. Comparing it to various state-of-the-art baselines, we demonstrated its superior performance on a wide range of continuous control benchmarks with various delayed and sparse reward patterns.

PBAC’s performance is sensitive to hyperparameters especially in dense reward environments. This is expected as it is designed to perform deep exploration in sparse-reward settings. While performing competitively in two dense environments, *ant* and *hopper*, it struggles in the dense *humanoid* as do several of the baselines. This is due to the significant amount of reward an agent receives by only remaining alive ($r = 5$) compared to $r = 1$ in the other two dense environments. It is not surprising that in this situation random exploration is sufficient and more robust. However, as soon as the reward becomes delayed, PBAC remains the only method to learn the task.

Our current work does not provide any convergence guarantees on PBAC’s behavior. This theoretical problem requires, and deserves, dedicated investigation. As PBAC builds on a sum of two Bellman backups and a regularizer, it will inherit similar properties to the guarantees of stochastic iterative Q -learning variants. Generalization of these guarantees to continuous state spaces is known to be a nontrivial problem which we consciously keep outside our focus.

Impact Statement

This paper presents work whose goal is to advance the field of Machine Learning. There are many potential societal consequences of our work, none which we feel must be specifically highlighted here.

References

- Agarwal, R., Schwarzer, M., Castro, P., Courville, A., and Bellemare, M. Deep reinforcement learning at the edge of the statistical precipice. *Advances in Neural Information Processing Systems (NeurIPS)*, 2021.
- Alquier, P. User-friendly introduction to PAC-Bayes bounds. *Foundations and Trends in Machine Learning*, 2024.
- Ambroladze, A., Parrado-Hernandez, E., and Shawe-Taylor, J. Tighter PAC-Bayes bounds. In *Advances in Neural Information Processing Systems (NeurIPS)*, 2006.
- Amin, S., Gomrokchi, M., Aboutaleb, H., Satija, H., and Precup, D. Locally persistent exploration in continuous control tasks with sparse rewards. In *Proceedings of the International Conference on Machine Learning (ICML)*, 2021.
- Ball, P., Smith, L., Kostrikov, I., and Levine, S. Efficient online reinforcement learning with offline data. In *Proceedings of the International Conference on Machine Learning (ICML)*, 2023.
- Bertsekas, D. and Tsitsiklis, J. *Neuro-dynamic programming*. Athena Scientific, 1996.
- Blei, D., Kucukelbir, A., and McAuliffe, J. Variational inference: A review for statisticians. *Journal of the American Statistical Association*, 2017.
- Boucheron, S., Lugosi, G., and Massart, P. *Concentration Inequalities: A Nonasymptotic Theory of Independence*. Oxford University Press, 02 2013. ISBN 9780199535255. doi: 10.1093/acprof:oso/9780199535255.001.0001. URL <https://doi.org/10.1093/acprof:oso/9780199535255.001.0001>.
- Brockman, G. Openai gym. *arXiv preprint arXiv:1606.01540*, 2016.
- Burda, Y., Edwards, H., Storkey, A., and Klimov, O. Exploration by random network distillation. In *International Conference on Learning Representations (ICLR)*, 2019.
- Catoni, O. PAC-Bayesian supervised classification: The thermodynamics of statistical learning. *Lecture Notes-Monograph Series*, 2007.
- Chentanez, N., Barto, A., and Singh, S. Intrinsically motivated reinforcement learning. In *Advances in Neural Information Processing Systems (NeurIPS)*, 2004.
- Chernoff, H. A Measure of Asymptotic Efficiency for Tests of a Hypothesis Based on the sum of Observations. *The Annals of Mathematical Statistics*, 23(4):493 – 507, 1952. doi: 10.1214/aoms/1177729330. URL <https://doi.org/10.1214/aoms/1177729330>.
- Cox, D. and Hinkley, D. *Theoretical Statistics*. Chapman & Hall, 1974.
- Curi, S., Berkenkamp, F., and Krause, A. Efficient model-based reinforcement learning through optimistic policy search and planning. In *Advances in Neural Information Processing Systems (NeurIPS)*, 2020.
- Donsker, M. D. and Varadhan, S. S. Asymptotic evaluation of certain markov process expectations for large time—iii. *Communications on pure and applied Mathematics*, 29 (4):389–461, 1976.
- Dziugaite, G. and Roy, D. Computing non-vacuous generalization bounds for deep (stochastic) neural networks with many more parameters than training data. In *Proceedings of the Conference on Uncertainty in Artificial Intelligence (UAI)*, 2017.
- Dziugaite, G. and Roy, D. Data-dependent PAC-Bayes priors via differential privacy. In *Advances in Neural Information Processing Systems (NeurIPS)*, 2018.
- Fan, J., Jiang, B., and Sun, Q. Hoeffding’s inequality for general markov chains and its applications to statistical learning. *Journal of Machine Learning Research (JMLR)*, 2021.
- Fard, M., Pineau, J., and Szepesvári, C. PAC-Bayesian policy evaluation for reinforcement learning. In *Proceedings on the International Conference on Artificial Intelligence and Statistics (AISTATS)*, 2012.
- Fellows, M., Hartikainen, K., and Whiteson, S. Bayesian Bellman operators. In *Advances in Neural Information Processing Systems (NeurIPS)*, 2021.
- Fellows, M., Kaplowitz, B., Schroeder de Witt, C., and Whiteson, S. Bayesian Exploration networks. In *Proceedings of the International Conference on Machine Learning (ICML)*, 2024.
- Flash, T. and Hochner, B. Motor primitives in vertebrates and invertebrates. *Current Opinion in Neurobiology*, 2005.
- Fortunato, M., Azar, M., Piot, B., Menick, J., Osband, I., Graves, A., Mnih, V., Munos, R., Hassabis, D., Pietquin,

- O., Blundell, C., and Legg, S. Noisy networks for exploration. In *International Conference on Learning Representations (ICLR)*, 2018.
- Fu, Y., Zhang, H., Wu, D., Xu, W., and Boulet, B. Furl: Visual-language models as fuzzy rewards for reinforcement learning. *arXiv preprint arXiv:2406.00645*, 2024.
- Fujimoto, S., Hoof, H., and Meger, D. Addressing function approximation error in actor-critic methods. In *Proceedings of the International Conference on Machine Learning (ICML)*, 2018.
- Germain, P., Lacasse, A., Laviolette, F., and Marchand, M. PAC-Bayesian learning of linear classifiers. In *Proceedings of the International Conference on Machine Learning (ICML)*, 2009.
- Grande, R., Walsh, T., and How, J. Sample efficient reinforcement learning with gaussian processes. In *Proceedings of the International Conference on Machine Learning (ICML)*, 2014.
- Guo, Z., Thakoor, S., Pšilar, M., Avila Pires, B., Altché, F., Tallec, C., Saade, A., Calandriello, D., Grill, J., Tang, Y., et al. Byol-explore: Exploration by bootstrapped prediction. *Advances in Neural Information Processing Systems (NeurIPS)*, 2022.
- Haarnoja, T., Zhou, A., Abbeel, P., and Levine, S. Soft Actor-Critic: Off-policy maximum entropy deep reinforcement learning with a stochastic actor. In *Proceedings of the International Conference on Machine Learning (ICML)*, 2018a.
- Haarnoja, T., Zhou, A., Hartikainen, K., Tucker, G., Ha, S., Tan, J., Kumar, V., Zhu, H., Gupta, A., Abbeel, P., et al. Soft actor-critic algorithms and applications. *arXiv preprint arXiv:1812.05905*, 2018b.
- Houthoofd, R., Chen, X., Duan, Y., Schulman, J., De Turck, F., and Abbeel, P. Vime: Variational information maximizing exploration. *Advances in Neural Information Processing Systems (NeurIPS)*, 2016.
- Jarrett, D., Tallec, C., Altché, F., Mesnard, T., Munos, R., and Valko, M. Curiosity in hindsight: Intrinsic exploration in stochastic environments. *Proceedings of the International Conference on Machine Learning (ICML)*, 2023.
- Kingma, D. and Ba, J. Adam: A method for stochastic optimization. In *International Conference on Learning Representations (ICLR)*, 2015.
- Kirk, D. *Optimal Control Theory: An Introduction*. Courier Corporation, 2004.
- Lakshminarayanan, B., Pritzel, A., and Blundell, C. Simple and scalable predictive uncertainty estimation using deep ensembles. *Advances in Neural Information Processing Systems (NeurIPS)*, 2017.
- Lillicrap, T., Hunt, J., Pritzel, A., Heess, N., Erez, T., Tassa, Y., Silver, D., and Wierstra, D. Continuous control with deep reinforcement learning. In *International Conference on Learning Representations (ICLR)*, 2016.
- Lipton, Z., Li, X., Gao, J., Li, L., Faisal, A., and Deng, L. BBQ-Networks: Efficient exploration in deep reinforcement learning for task-oriented dialogue systems. In *Proceedings of the AAAI Conference on Artificial Intelligence*, 2018.
- Luis, C., Bottero, A., Vinogradskaja, J., Berkenkamp, F., and Peters, J. Model-based uncertainty in value functions. In *Proceedings on the International Conference on Artificial Intelligence and Statistics (AISTATS)*, 2023a.
- Luis, C., Bottero, A. G., Vinogradskaja, J., Berkenkamp, F., and Peters, J. Value-distributional model-based reinforcement learning. *arXiv preprint arXiv:2308.06590*, 2023b.
- Mazouze, B., Doan, T., Durand, A., Hjelm, R., and Pineau, J. Leveraging exploration in off-policy algorithms via normalizing flows. In *Conference on Robot Learning (CoRL)*, 2019.
- McAllester, D. PAC-Bayesian model averaging. In *Proceedings of the Conference on Learning Theory (COLT)*, 1999.
- Modirshanechi, A., Kondrakiewicz, K., Gerstner, W., and Haesler, S. Curiosity-driven exploration: foundations in neuroscience and computational modeling. *Trends in Neurosciences*, 2023.
- Nauman, M., Bortkiewicz, M., Miłoś, P., Trzcinski, T., Ostaszewski, M., and Cygan, M. Overestimation, overfitting, and plasticity in actor-critic: the bitter lesson of reinforcement learning. In *Proceedings of the International Conference on Machine Learning (ICML)*, 2024.
- Nikulin, A., Kurenkov, V., Tarasov, D., and Kolesnikov, S. Anti-exploration by random network distillation. In *Proceedings of the International Conference on Machine Learning (ICML)*, 2023.
- Osband, I., Russo, D., and Van Roy, B. (more) efficient reinforcement learning via posterior sampling. *Advances in Neural Information Processing Systems (NeurIPS)*, 2013.
- Osband, I., Blundell, C., Pritzel, A., and Van Roy, B. Deep exploration via bootstrapped DQN. *Advances in Neural Information Processing Systems (NeurIPS)*, 2016a.

- Osband, I., Van Roy, B., and Wen, Z. Generalization and exploration via randomized value functions. In *Proceedings of the International Conference on Machine Learning (ICML)*, 2016b.
- Osband, I., Aslanides, J., and Cassirer, A. Randomized prior functions for deep reinforcement learning. In *Advances in Neural Information Processing Systems (NeurIPS)*, 2018.
- O’Donoghue, B., Osband, I., Munos, R., and Mnih, V. The uncertainty bellman equation and exploration. In *Proceedings of the International Conference on Machine Learning (ICML)*, 2018.
- Paszke, A., Gross, S., Massa, F., Lerer, A., Bradbury, J., Chanan, G., Killeen, T., Lin, Z., Gimelshein, N., Antiga, L., Desmaison, A., Kopf, A., Yang, E., DeVito, Z., Raison, M., Tejani, A., Chilamkurthy, S., Steiner, B., Fang, L., Bai, J., and Chintala, S. PyTorch: An Imperative Style, High-Performance Deep Learning Library. *Advances in Neural Information Processing Systems (NeurIPS)*, 2019.
- Plappert, M., Houthoofd, R., Dhariwal, P., Sidor, S., Chen, R., Chen, X., Asfour, A., Abbeel, P., and Andrychowicz, M. Parameter space noise for exploration. In *International Conference on Learning Representations (ICLR)*, 2018.
- Polyanskiy, Y. and Wu, Y. Lecture notes on information theory. *UIUC*, 2014.
- Puterman, M. *Markov decision processes: discrete stochastic dynamic programming*. John Wiley & Sons, 2014.
- Reeb, D., Doerr, A., Gerwin, S., and Rakitsch, B. Learning Gaussian processes by minimizing PAC-Bayesian generalization bounds. *Advances in Neural Information Processing Systems (NeurIPS)*, 2018.
- Rudner, T., Chen, Z., Teh, Y., and Gal, Y. Tractable function-space variational inference in Bayesian neural networks. *Advances in Neural Information Processing Systems (NeurIPS)*, 2022.
- Schaal, S. Dynamic movement primitives -a framework for motor control in humans and humanoid robotics. *Adaptive Motion of Animals and Machines*, 2006.
- Schmidhuber, J. Formal theory of creativity, fun, and intrinsic motivation (1990–2010). *IEEE Transactions on Autonomous Mental Development*, 2010.
- Seeger, M. PAC-Bayesian generalisation error bounds for Gaussian process classification. *Journal of Machine Learning Research (JMLR)*, 2002.
- Shang, W., Sohn, K., Almeida, D., and Lee, H. Understanding and improving convolutional neural networks via concatenated rectified linear units. In *Proceedings of the International Conference on Machine Learning (ICML)*, 2016.
- Shawe-Taylor, J. and Williamson, R. A PAC analysis of Bayesian estimator. In *Proceedings of the Conference on Learning Theory (COLT)*, 1997.
- Silver, D., Hubert, T., Schrittwieser, J., Antonoglou, I., Lai, M., Guez, A., Lanctot, M., Sifre, L., Kumaran, D., Graepel, T., Lillicrap, T., Simonyan, K., and Hassabis, D. A general reinforcement learning algorithm that masters chess, shogi, and go through self-play. *Science*, 2018.
- Stengel, R. *Optimal Control and Estimation*. Courier Corporation, 1994.
- Strens, M. A Bayesian framework for reinforcement learning. In *Proceedings of the International Conference on Machine Learning (ICML)*, 2000.
- Sun, Y., Zhang, J., Jia, C., Lin, H., Ye, J., and Yu, Y. Model-Bellman inconsistency for model-based offline reinforcement learning. In *Proceedings of the International Conference on Machine Learning (ICML)*, 2023.
- Tasdighi, B., Akgül, A., Haussmann, M., Brink, K. K., and Kandemir, M. PAC-Bayesian soft actor-critic learning. In *Advances in Approximate Bayesian Inference (AABI)*, 2024.
- Tassa, Y., Doron, Y., Muldal, A., Erez, T., Li, Y., Casas, D. d. L., Budden, D., Abdolmaleki, A., Merel, J., Lefrancq, A., et al. Deepmind control suite. *arXiv preprint arXiv:1801.00690*, 2018.
- Thrun, S. and Schwartz, A. Issues in using function approximation for reinforcement learning. In *Proceedings of the Fourth Connectionist Models Summer School*, 1993.
- Todorov, E., Erez, T., and Tassa, Y. Mujoco: A physics engine for model-based control. In *IEEE/RSJ International Conference on Intelligent Robots and Systems (IROS)*, 2012.
- Touati, A., Satija, H., Romoff, J., Pineau, J., and Vincent, P. Randomized value functions via multiplicative normalizing flows. In *Uncertainty in Artificial Intelligence (UAI)*, 2020.
- Towers, M., Kwiatkowski, A., Terry, J., Balis, J., De Cola, G., Deleu, T., Goulão, M., Kallinteris, A., Krimmel, M., KG, A., et al. Gymnasium: A standard interface for reinforcement learning environments. *arXiv preprint arXiv:2407.17032*, 2024.
- Van Hasselt, H. Double Q-learning. *Advances in Neural Information Processing Systems (NeurIPS)*, 2010.

Wu, Y.-S., Zhang, Y., Chérief-Abdellatif, B.-E., and Seldin, Y. Recursive PAC-Bayes: A frequentist approach to sequential prior updates with no information loss. In *Advances in Neural Information Processing Systems (NeurIPS)*, 2024.

Yang, K., Tao, J., Lyu, J., and Li, X. Exploration and anti-exploration with distributional random network distillation. In *Proceedings of the International Conference on Machine Learning (ICML)*, 2024.

Yu, T., Quillen, D., He, Z., Julian, R., Hausman, K., Finn, C., and Levine, S. Meta-world: A benchmark and evaluation for multi-task and meta reinforcement learning. In *Conference on Robot Learning (CoRL)*, 2020a.

Yu, T., Thomas, G., Yu, L., Ermon, S., Zou, J., Levine, S., Finn, C., and Ma, T. MOPO: Model-based offline policy optimization. *Advances in Neural Information Processing Systems (NeurIPS)*, 2020b.

APPENDIX

In this appendix, we include proofs and derivations for all theoretical statements made in the main text in Section A. Section A.1.1 contains a short discussion on differences between our bound and Fard et al. (2012)'s result. We summarize all experimental details and a pseudo code algorithm for our model in Sections B and C. Section D closes the appendix with a series of further results and ablations.

A. Proofs and derivations

For practical purposes, we assume in the proofs that all probability measures except ρ have densities. The proofs can be straightforwardly extended by lifting this assumption. To prove our main theorem, we require the following three lemmas.

Lemma 1. For any ρ defined on X , the following identity holds

$$\tilde{L}(\rho) = \mathbb{E}_{X \sim \rho} \|T_\pi X - X\|_{P_\pi}^2 + \gamma^2 \mathbb{E}_{X \sim \rho} [\text{Var}_{s \sim P_\pi} [X(s, \pi(s))]].$$

Proof of Lemma 1. For a fixed X we have

$$\begin{aligned} \tilde{L}(X) &= \mathbb{E}_{s \sim P_\pi} \left[\mathbb{E}_{s' \sim P(\cdot | s, \pi(s))} \left[\left(\tilde{T}_\pi X(s, \pi(s), s') - X(s, \pi(s)) \right)^2 \middle| s \right] \right] \\ &= \mathbb{E}_{s \sim P_\pi} \left[\mathbb{E}_{s' \sim P(\cdot | s, \pi(s))} \left[\tilde{T}_\pi X(s, \pi(s), s')^2 + X(s, \pi(s))^2 - 2\tilde{T}_\pi X(s, \pi(s), s')X(s, \pi(s)) \middle| s \right] \right] \\ &= \mathbb{E}_{s \sim P_\pi} \left[\mathbb{E}_{s' \sim P(\cdot | s, \pi(s))} \left[\tilde{T}_\pi X(s, \pi(s), s')^2 \middle| s \right] \right. \\ &\quad \left. + X(s, \pi(s))^2 - 2\mathbb{E}_{s' \sim P(\cdot | s, \pi(s))} \left[\tilde{T}_\pi X(s, \pi(s), s') \middle| s \right] X(s, \pi(s)) \right] \\ &= \mathbb{E}_{s \sim P_\pi} \left[\mathbb{E}_{s' \sim P(\cdot | s, \pi(s))} \left[\tilde{T}_\pi X(s, \pi(s), s') \middle| s \right]^2 \right. \\ &\quad \left. + \text{Var}_{s' \sim P(\cdot | s, \pi(s))} \left[\tilde{T}_\pi X(s, \pi(s), s') \middle| s \right] + X(s, \pi(s))^2 \right. \\ &\quad \left. - 2\mathbb{E}_{s' \sim P(\cdot | s, \pi(s))} \left[\tilde{T}_\pi X(s, \pi(s), s') \middle| s \right] X(s, \pi(s)) \right] \\ &= \mathbb{E}_{s \sim P_\pi} \left[\left(\mathbb{E}_{s' \sim P(\cdot | s, \pi(s))} \left[\tilde{T}_\pi X(s, \pi(s), s') \middle| s \right] - X(s, \pi(s)) \right)^2 + \text{Var}_{s' \sim P(\cdot | s, \pi(s))} \left[\tilde{T}_\pi X(s, \pi(s), s') \middle| s \right] \right] \\ &= \mathbb{E}_{s \sim P_\pi} \left[\left(T_\pi X(s, \pi(s)) - X(s, \pi(s)) \right)^2 + \text{Var}_{s' \sim P(\cdot | s, \pi(s))} \left[\tilde{T}_\pi X(s, \pi(s), s') \middle| s \right] \right] \\ &= \|T_\pi X - X\|_{P_\pi}^2 + \mathbb{E}_{s \sim P_\pi} \left[\text{Var}_{s' \sim P(\cdot | s, \pi(s))} \left[\tilde{T}_\pi X(s, \pi(s), s') \middle| s \right] \right] \\ &= \|T_\pi X - X\|_{P_\pi}^2 + \mathbb{E}_{s \sim P_\pi} \left[\text{Var}_{s' \sim P(\cdot | s, \pi(s))} [r(s, \pi(s)) + \gamma X(s', \pi(s')) \middle| s] \right] \\ &= \|T_\pi X - X\|_{P_\pi}^2 + \gamma^2 \mathbb{E}_{s \sim P_\pi} \left[\text{Var}_{s' \sim P(\cdot | s, \pi(s))} [X(s', \pi(s')) \middle| s] \right]. \end{aligned}$$

Since the Markov process is stationary we get

$$\mathbb{E}_{s \sim P_\pi} \left[\mathbb{E}_{s' \sim P(\cdot | s, \pi(s))} [X(s', \pi(s')) \middle| s] \right] = \mathbb{E}_{s \sim P_\pi} [X(s, \pi(s))]$$

as well as

$$\mathbb{E}_{s \sim P_\pi} \left[\mathbb{E}_{s' \sim P(\cdot | s, \pi(s))} [X(s', \pi(s'))^2 \middle| s] \right] = \mathbb{E}_{s \sim P_\pi} [X(s, \pi(s))^2].$$

Hence, the variance term can be expressed as

$$\begin{aligned} \mathbb{E}_{s \sim P_\pi} \left[\text{Var}_{s' \sim P(\cdot | s, \pi(s))} [X(s', \pi(s')) \middle| s] \right] &= \mathbb{E}_{s \sim P_\pi} [X(s, \pi(s))^2] - \mathbb{E}_{s \sim P_\pi} [X(s, \pi(s))]^2 \\ &= \text{Var}_{s \sim P_\pi} [X(s, \pi(s))]. \end{aligned}$$

Taking the expectation over X with respect to ρ concludes the proof. \square

Lemma 2. For any $Q_1, Q_2 : \mathcal{S} \times \mathcal{A} \rightarrow \mathbb{R}$ and stationary state visitation distribution P_π , the following inequality holds:

$$\|T_\pi Q_1 - T_\pi Q_2\|_{P_\pi} \leq \gamma \|Q_1 - Q_2\|_{P_\pi}.$$

That is, the Bellman operator T_π is a γ -contraction with respect to the P_π -weighted L_2 -norm $\|\cdot\|_{P_\pi}$

Proof of Lemma 2.

$$\begin{aligned} \|T_\pi Q_1 - T_\pi Q_2\|_{P_\pi}^2 &= \mathbb{E}_{s \sim P_\pi} \left[\left(T_\pi Q_1(s, \pi(s)) - T_\pi Q_2(s, \pi(s)) \right)^2 \right] \\ &= \gamma^2 \mathbb{E}_{s \sim P_\pi} \left[\left(\mathbb{E}_{s' \sim P(\cdot|s, \pi(s))} [T_\pi Q_1(s', \pi(s')) - T_\pi Q_2(s', \pi(s')) | s] \right)^2 \right] \\ &\leq \gamma^2 \mathbb{E}_{s \sim P_\pi} \left[\mathbb{E}_{s' \sim P(\cdot|s, \pi(s))} \left[\left(T_\pi Q_1(s', \pi(s')) - T_\pi Q_2(s', \pi(s')) \right)^2 | s \right] \right] && \text{(Jensen)} \\ &= \gamma^2 \mathbb{E}_{s' \sim P_\pi} \left[\left(T_\pi Q_1(s', \pi(s')) - T_\pi Q_2(s', \pi(s')) \right)^2 \right]. && \text{(Stationarity)} \end{aligned}$$

Taking the square-root of both sides yields the result. \square

Lemma 3. For any ρ defined on X the following inequality holds:

$$\mathbb{E}_{X \sim \rho} \|X - Q_\pi\|_{P_\pi} \leq \frac{\mathbb{E}_{X \sim \rho} \|T_\pi X - X\|_{P_\pi}}{1 - \gamma}.$$

Proof of Lemma 3. For any fixed X we have

$$\begin{aligned} \|X - Q_\pi\|_{P_\pi} &= \|X - T_\pi X + T_\pi X - Q_\pi\|_{P_\pi} \\ &= \|X - T_\pi X + T_\pi X - T_\pi Q_\pi\|_{P_\pi} \\ &\leq \|X - T_\pi X\|_{P_\pi} + \|T_\pi X - T_\pi Q_\pi\|_{P_\pi} && \text{(Triangle ineq.)} \\ &\leq \|X - T_\pi X\|_{P_\pi} + \gamma \|X - Q_\pi\|_{P_\pi}. && \text{(Lemma 2)} \end{aligned}$$

Rearranging the terms and integrating over all X 's weighted by ρ yields the result. \square

Theorem 2. For any posterior and prior measures $\rho, \rho_0 \in \mathcal{P}$, error tolerance $\delta \in (0, 1]$, and deterministic policy π , simultaneously, the following inequality holds with probability at least $1 - \delta$:

$$\mathbb{E}_{X \sim \rho} \|Q_\pi - X\|_{P_\pi}^2 \leq \left(\widehat{L}_D(\rho) + \frac{\nu \bar{\lambda} B^2}{8n} + \frac{\text{KL}(\rho \| \rho_0) - \log \delta}{\nu} - \gamma^2 \mathbb{E}_{X \sim \rho} \text{Var}_{s \sim P_\pi} [X(s, \pi(s))] \right) / (1 - \gamma)^2$$

where $\bar{\lambda} \triangleq \frac{1 + \max_{t \in [n]} \lambda_t}{1 - \max_{t \in [n]} \lambda_t}$, with $\lambda_t \in [0, 1)$ as the operator norm of the transition kernel of the time-inhomogeneous Bellman error Markov chain at time t , $B = R^2 / (1 - \gamma)^2$ and $\nu > 0$ an arbitrary constant.

To prove this theorem, we rely on the following result by [Fan et al. \(2021\)](#), which we quote below.⁵

Theorem (Fan et al., 2021). Consider a time-inhomogeneous Markov chain π -stationary Markov chain $\{X_i\}_{i \geq 1}$. If its transition probability kernel P_i admits absolute spectral gap $1 - \lambda_i, \forall i \geq 1$, then, for any bounded function $f_i : \mathcal{X} \rightarrow [a_i, b_i]$, the sum $\sum_i f_i(X_i)$ is sub-Gaussian with variance proxy

$$\sigma^2 \leq \frac{1 + \max_i \lambda_i}{1 - \max_i \lambda_i} \sum_i \frac{(b_i - a_i)^2}{4}.$$

We partially follow [Alquier \(2024\)](#)'s proof on the Catoni bound adapting it to our specific setup.⁶

⁵Theorem 5 in [Fan et al. \(2021\)](#).

⁶Section 2.1 in [Alquier \(2024\)](#).

Proof of Theorem 2. Consider the Bellman error as a time-inhomogeneous Markov chain, $\{X_t \triangleq (\tilde{T}_{\pi_t}(X(s_t, \pi_t(s_t), s_{t+1})) - X(s_t, a_t))\}_{t \geq 1}$, whose state transition kernel has an absolute spectral gap $1 - \lambda_t$ for each $t \geq 1$.⁷ Let $\bar{\lambda} \triangleq (1 + \max_{t \in [n]} \lambda_t) / (1 - \max_{t \in [n]} \lambda_t)$. For a bounded function $f : \mathcal{X} \rightarrow [0, B]$, we have with Fan et al. (2021) that $\sum_t f(X_t)$ is sub-Gaussian⁸ with variance proxy

$$\sigma^2 \leq \bar{\lambda} \frac{nB^2}{4}.$$

Defining $F_n \triangleq \frac{1}{n} \sum_t f(X_t)$, we therefore have

$$\mathbb{E} [\exp(\nu (F_n - \mathbb{E}[F_n]))] \leq \exp\left(\frac{\bar{\lambda} B^2 \nu^2}{8n}\right).$$

Integrating both sides with respect to ρ_0 and applying Fubini's theorem gives us

$$\mathbb{E}_{\mathcal{D}} [\mathbb{E}_{\rho_0} [\exp(\nu (\mathbb{E}[F_n] - F_n))]] \leq \exp\left(\frac{\nu^2 \bar{\lambda} B^2}{8n}\right),$$

where $\mathbb{E}_{\mathcal{D}}$ is the expectation over the data set \mathcal{D} . Applying Donsker and Varadhan's variational formula (Donsker & Varadhan, 1976), we get that

$$\mathbb{E}_{\mathcal{D}} \left[\exp \left(\sup_{\rho} \left(\nu \mathbb{E}_{\rho} [\mathbb{E}[F_n] - F_n] - \text{KL}(\rho \parallel \rho_0) \right) \right) \right] \leq \exp \left(\frac{\nu^2 \bar{\lambda} B^2}{8n} \right).$$

With $f(x) = x^2$, we have that $B = R^2 / (1 - \gamma)^2$ and can rewrite the inequality in terms of $L(\rho)$ and $\hat{L}(\rho)$, such that

$$\mathbb{E}_{\mathcal{D}} \left[\exp \left(\sup_{\rho} \left(\nu (L(\rho) - \hat{L}_{\mathcal{D}}(\rho)) - \text{KL}(\rho \parallel \rho_0) \right) - \frac{\nu^2 \bar{\lambda} B^2}{8n} \right) \right] \leq 1.$$

With Chernoff's bound (Chernoff, 1952) we have for a fixed $s > 0$

$$\begin{aligned} & \mathbb{P}_{\mathcal{D}} \left(\sup_{\rho} \left(\nu (L(\rho) - \hat{L}_{\mathcal{D}}(\rho)) - \text{KL}(\rho \parallel \rho_0) \right) - \frac{\nu^2 \bar{\lambda} B^2}{8n} > s \right) \\ & \leq \mathbb{E}_{\mathcal{D}} \left[\exp \left(\sup_{\rho} \left(\nu (L(\rho) - \hat{L}_{\mathcal{D}}(\rho)) - \text{KL}(\rho \parallel \rho_0) \right) - \frac{\nu^2 \bar{\lambda} B^2}{8n} \right) \right] e^{-s} \leq e^{-s}. \end{aligned}$$

With a choice of $s = \log(1/\delta)$ and rearranging the terms we get that with probability smaller than δ

$$\sup_{\rho} \left(\nu (L(\rho) - \hat{L}_{\mathcal{D}}(\rho)) - \text{KL}(\rho \parallel \rho_0) \right) - \frac{\nu^2 \bar{\lambda} B^2}{8n} > \log \frac{1}{\delta},$$

that is, for all ρ

$$L(\rho) \leq \hat{L}(\rho) + \frac{\nu \bar{\lambda} B^2}{8n} + \frac{\text{KL}(\rho \parallel \rho_0) - \log \delta}{\nu}, \quad (5)$$

with probability $1 - \delta$. Finally, with Lemma 1 we have that

$$\mathbb{E}_{X \sim \rho} [\|T_{\pi} X - X\|_{P_{\pi}}^2] \leq \hat{L}(\rho) + \frac{\nu \bar{\lambda} B^2}{8n} + \frac{\text{KL}(\rho \parallel \rho_0) - \log \delta}{\nu} - \gamma^2 \mathbb{E}_{X \sim \rho} \text{Var}_{s \sim P_{\theta}} [X(s, \pi(s))],$$

and applying Lemma 3 on the left-hand side gives the claimed inequality. \square

⁷Note, this transition kernel differs from the environmental kernel P .

⁸A random variable X is sub-Gaussian with variance proxy σ^2 if $\mathbb{E}[X]$ is finite and $\mathbb{E}[\exp(t(X - \mathbb{E}[X]))] \leq \exp(\sigma^2 t^2 / 2)$ for all $t \in \mathbb{R}$ (Boucheron et al., 2013).

A.1. Discussion on the bound

We close this section with a series of remarks on the theorem.

- (i) *The chain $\{X_i\}$ and f_i .* While we focused on the Bellman error and a squared function $f = f_i(x) = x^2$, the proof can be trivially adapted to other chains and bounded functions.
- (ii) *The spectral gap factor $\bar{\lambda}$.* As $\max_t \lambda_t \rightarrow 1$, $\bar{\lambda} \rightarrow \infty$. However, this implies increasing auto-correlation in the transition kernel, which we consider to be unrealistic in practice.
- (iii) *The bound B^2 .* The bound of f appears squared in the final bound, i.e., $B^2 = R^4/(1 - \gamma)^4$. Depending on R and the choice of $\gamma \in (0, 1)$ its influence could be large. This is mitigated in practice as the related term disappears with $n \rightarrow \infty$ or $\nu \rightarrow 0$. Note that the choice of ν is arbitrary. Theorem 2.4 together with Corollary 2.5 from [Alquier \(2024\)](#) extend the bound with an infimum over a discretized grid of ν values.
- (iv) *A justification for minimizing the right-hand side of the bound.* Corollary 2.3 in [Alquier \(2024\)](#) shows that the Gibbs posterior, $\hat{\rho}_\nu = \arg \min_\rho \left(\hat{L}(\rho) + \text{KL}(\rho \parallel \rho_0) / \nu \right)$ minimizes the right-hand side of the bound. Therefore we have that

$$\mathbb{P} \left(L(\hat{\rho}_\nu) \leq \inf_\rho \left(\hat{L}(\rho) + \frac{\nu \bar{\lambda} B^2}{8n} + \frac{\text{KL}(\rho \parallel \rho_0) - \log \delta}{\nu} \right) \right) \geq 1 - \delta,$$

which justifies our choice of using the right-hand side of the bound as our training objective.

A.1.1. DERIVATION OF A RELATED BOUND.

We conclude the discussion on the generalization bound with an alternative we get by adapting [Fard et al. \(2012\)](#).

Using the sub-Gaussianity theorem by [Fan et al. \(2021\)](#) cited above, we have the following result.

Corollary. *Assuming a Markov chain $\{X_i\}_{i \geq 1}$ and bounded functions f_i following the assumptions of Theorem 5 by [Fan et al. \(2021\)](#) we have that*

$$\mathbb{P} \left(\sum_i f_i(X_i) - \sum_i \mathbb{E}[f_i(X_i)] \geq \varepsilon \right) \leq \exp \left(-\frac{\varepsilon^2}{2\bar{\lambda} \sum_i (b_i - a_i)^2 / 4} \right),$$

where $\bar{\lambda} = \frac{1 + \max_i \lambda_i}{1 - \max_i \lambda_i}$ and $\varepsilon > 0$. Equivalently,

$$\sum_i f_i(X_i) - \sum_i \mathbb{E}[f_i(X_i)] \leq \sqrt{\bar{\lambda} \sum_i (b_i - a_i)^2 / 2 \log(1/\delta)},$$

with probability $1 - \delta$ where $\delta \in (0, 1)$.

The result follows after a straight forward application of Chernoff's bound using the sub-Gaussianity of $\sum_i f_i$.

Assuming $f = f_i$ for all i , i.e., and $f(X) \in [0, B]$, we can further simplify the result of the corollary to

$$\frac{1}{n} \sum_i f(X_i) - \frac{1}{n} \sum_i \mathbb{E}[f(X_i)] \leq \sqrt{\frac{\bar{\lambda} B^2}{2n} \log(1/\delta)},$$

with probability $1 - \delta$. Assuming a sufficiently large amount of observations, such that $n > \bar{\lambda} B^2 / 2$, the assumptions of [Fard et al. \(2012\)](#)'s Theorem 1 hold and we have, with probability $1 - \delta$, that

$$\frac{1}{n} \sum_i f(X_i) - \frac{1}{n} \sum_i \mathbb{E}[f(X_i)] \leq \sqrt{\frac{\log(2n/\bar{\lambda} B^2) - \log \delta + \text{KL}(\rho \parallel \rho_0)}{2n/\bar{\lambda} B^2 - 1}},$$

where ρ and ρ_0 are distributions over a measurable hypothesis space \mathcal{F} and $f \in \mathcal{F}$. Compared with the bound in (5) it suffers from the constraint on the number of data points. As $n > R^4/(1 - \gamma)^4$ will rarely be fulfilled in practice for typical values of γ , e.g., $\gamma = 0.99$ in our paper, it cannot be used as a theoretically justified training objective. However, if its constraints were fulfilled, we can use their approach to get a tighter generalization bound.

A.2. Derivation of the approximation to the KL divergence term

$$\begin{aligned}
 \text{KL}(\rho(s, \pi(s)) || \rho_0(s, \pi(s))) &\approx \mathbb{E}_{X \sim \rho} [\log f_\rho(X|s, a) - \log f_{\rho_0}(X|s, a)] \\
 &\approx \frac{1}{K} \sum_{k=1}^K \log f_\rho(X_k|s, \pi_k(s)) - \log f_{\rho_0}(X_k|s, \pi_k(s)) \\
 &= \frac{1}{2} \frac{1}{K} \sum_{k=1}^K \left(-\log \sigma_\pi^2(s) - \frac{(r + \gamma \mu_\pi(s) - X_k)^2}{\sigma_\pi^2(s)} + \log(\gamma^2 \sigma_0^2) + \frac{(r + \gamma \bar{\mu}_\pi(s') - X_k)^2}{\gamma^2 \sigma_0^2} \right) \\
 &= \frac{1}{2} \left(-K \log \sigma_\pi^2(s) - \frac{1}{\sigma_\pi^2(s)} \underbrace{\frac{1}{K} \sum_{k=1}^K (r + \gamma \mu_\pi(s) - X_k)^2}_{=\frac{K-1}{K} \sigma_\pi^2(s)} + K \log(\gamma^2 \sigma_0^2) + \frac{1}{K} \sum_{k=1}^K \frac{(r + \gamma \bar{\mu}_\pi(s') - X_k)^2}{\gamma^2 \sigma_0^2} \right) \\
 &= \frac{1}{2K} \sum_{k=1}^K \left(\frac{(r + \gamma \bar{\mu}_\pi(s') - X_k)^2}{\gamma^2 \sigma_0^2} - \log \sigma_\pi^2(s) \right) + \text{const.}
 \end{aligned}$$

B. Experimental details

B.1. Prior work on delayed rewards and reward sparsity in continuous control

How to structure a delayed reward environment is a matter of debate. We identify two broad groups of environments in the current state-of-the-art literature, without claiming this to be an exhaustive survey. These consist either of native, i.e., inherent sparsity in the original environment or are custom modifications of dense reward environments made by the respective authors. We follow the naming convention for each of the environments as used in the Gymnasium (Towers et al., 2024), DMControl (Tassa et al., 2018) and Meta-World (Yu et al., 2020a) libraries unless otherwise noted.

(i) Binary rewards based on proximity to a target state. Houthoof et al. (2016) and Fellows et al. (2021) study Mountain Car continuous and sparse cartpole swing up. Fellows et al. (2021) reach a reward of around 500 in cartpole within more than 1.5 million environment interactions, far behind the levels we report in our experiments. Curi et al. (2020) study reacher, pusher, a custom sparsified version of reacher with a reward squashed around the goal state and action penalty with an increased share. Houthoof et al. (2016), Mazouze et al. (2019), and Amin et al. (2021) sparsify various MuJoCo locomotors by granting binary reward based on whether the locomotor reaches a target x -coordinate. This reward design has limitations: (i) Since there is no action penalty, the locomotor does not need to aim at its actuators in the most efficient way, (ii) Since there is no forward reward proportional to velocity, the locomotor’s performance after reaching a target location becomes irrelevant. For instance, a humanoid can also fall down or stand still after reaching the target.

(ii) Increased action penalties. Curi et al. (2020) study cartpole and MuJoCo HalfCheetah with increased action penalties. Luis et al. (2023a) use pendulum swingup with nonzero reward only in the close neighborhood of the target angle. They also apply an action cost and perturb the pendulum angle with Gaussian white noise. They also report results on PyBullet Gym locomotors HalfCheetah, Walker2D, and Ant with dense rewards. Their follow-up work (Luis et al., 2023b) addresses a larger set of DMC environments where locomotors are customized to receive action penalties. The limitation of this reward design is that increasing the action penalty is not sufficient to sparsify the reward as the agent can still observe relative changes in the forward reward from its contributions to the total reward. In some MuJoCo variants, the agent also receives rewards on the health status, which is a signal about intermediate success against the sparse-reward learning goal. Furthermore, action penalties are typically exogenous factors determined by energy consumption in the real world, making the challenge artificial.

In Section 4, we report results on the most difficult subset of some natively sparse environments and devise new locomotion setups that overcome the aforementioned limitations. We discuss them in the next subsection.

Table 3. MuJoCo environment reward hyperparameters. See the description in the text for an explanation on each of the parameters.

TASK	Positional delay c	Action cost weight w_a	Health reward H
ant	0	5e-1	1
ant (delayed)	0	5e-1	0
ant (very delayed)	2	5e-1	0
hopper	0	1e-3	1
hopper (delayed)	0	1e-3	0
hopper (very delayed)	1	1e-3	0
humanoid	0	1e-1	5
humanoid (delayed)	0	1e-1	0

B.2. Experiment pipeline design

The whole experiment pipeline is implemented in PyTorch (Paszke et al., 2019, version 2.4.1). The experiments are conducted on eleven continuous control environments from two physics engines, MuJoCo (Todorov et al., 2012; Brockman, 2016) and DeepMind Control (DMControl) Suite (Tassa et al., 2018), along with further seven robotic tasks from sparse Meta-World (Yu et al., 2020a). All MuJoCo environments used are from version 4 of the MuJoCo suite (V4), and sparse DMControl environments. Multi-task sparse Meta-World environments are from version 2.

B.2.1. MUJoCo

From the two locomotors that can stand without control, we choose *ant* as it is defined on the 3D space compared to the 2D defined *halfcheetah*. From the two locomotors that have to learn to keep their balance, we choose *hopper* instead of *walker2d* as hopping is a more dexterous locomotion task than walking. We also choose *humanoid* as an environment where a 3D agent with a very large state and action space has to learn to keep its balance. The reward functions of the MuJoCo locomotion tasks have the following generic form:

$$r \triangleq \underbrace{\frac{dx_t}{dt}}_{\text{Forward reward}} - \underbrace{w_a \|a_t\|^2}_{\text{Action cost}} + \underbrace{H}_{\text{Health reward}}.$$

Forward reward comes from the motion speed of the agent towards its target direction and drives the agent to move efficiently toward the goal. *Health reward* is an intermediate incentive an agent receives to maintain its balance. The *action cost* ensure that the agent solves the task using minimum energy. We implement sparsity to the locomotion environments in the following two ways using the following reward function template:

$$r_{\text{delayed}} := \underbrace{\frac{dx_t}{dt} \mathbf{1}_{x_t > c}}_{\text{Forward reward}} - \underbrace{w_a \|a_t\|^2}_{\text{Action cost}}.$$

This function delays forward rewards until the center of mass of the locomotor x_t reaches a chosen target position c , which we call as the *positional delay*. This reward also removes the healthy reward to ensure that the agent does not get any incentive by solving an intermediate task. It is possible to increase the sparsity of a task by increasing the positional delay. Detailed information on the sparsity levels we used in our experiments are listed in Table 3. For each environment, we choose the largest positional delay, i.e. maximum sparsity, where at least one model can successfully solve the task. Beyond this threshold, all models fail to collect positive rewards within 300000 environment interactions. The structure of these experiments follows the same structure as what is known as the n -chains thought experiment, which is studied extensively in theoretical work. The essential property is that there is a long period of small reward on which an agent can overfit. See, e.g., the discussion by Strens (2000) or Osband et al. (2018) for further details. Information on the state and action space dimensionalities for each of the three environments is available in Table 4.

Table 4. State and action space dimensionalities for MuJoCo (MJC) and DMControl (DMC).

	TASK	$ \mathcal{S} $	$ \mathcal{A} $
MJC	ant	27	8
	hopper	11	3
	humanoid	376	17
DMC	ballincup	8	2
	cartpole	5	1
	reacher	11	2

B.2.2. DEEPMIND CONTROL

From DMControl, we choose *ballincup*, *cartpole*, and *reacher*, as they have sparse binary reward functions given based on task completion. In *ballincup*, the task is defined as whether the relative position of the ball to the cup centroid is below a distance threshold. In the *cartpole*, it is whether cart position and pole angle are in respective ranges $(-0.25, 0.25)$ and $(0.995, 1)$. Finally, in the *reacher*, it is the distance between the arm and the location of a randomly placed target coordinate. Information on the state and action space dimensionalities for each of the three environments is available in Table 4. We did not consider the DMC locomotors as they use the same physics engine as MuJoCo and their reward structure is less challenging due to the absence of the action penalty and the diminishing returns given to increased velocities.

B.2.3. META-WORLD

We conduct our experiments using robotic tasks from the multi-task Meta-World environment, originally introduced by Yu et al. (2020a) with sparse rewards where the agent receives a reward of one only by reaching the goal and zero otherwise. In all environments, the goal location is hidden. The experiments were conducted over 1 000 000 environment steps across five different seeds, with success rates evaluated for all baselines. Our experimental scheme follows Fu et al. (2024). Three environments were excluded from our evaluation compared to them because none of the baseline methods were able to solve these three tasks. These tasks are particularly challenging under sparse reward conditions, as they require mastering multiple subtasks which significantly increases the difficulty (Fu et al., 2024). See Table 5 for additional details on the hyperparameters. We provide a description of each task in Table 6. The area under success rate curve and final episode success rate results are summarized in Table 2 and visualized in Figure 3.

B.3. Evaluation methodology

Performance metrics. We calculate the *Interquartile Mean (IQM)* of the final episode reward and of the *area under learning curve (AULC)* as our performance scores where the former indicates how well the task has been solved and the latter is a measure of learning speed. The AULC is calculated using evaluation episodes after every 20 000 steps. We calculate these rewards over ten repetitions on different seeds, where each of the methods gets the same seeds. All methods, including our approach and the baselines, utilize the same warmup phase of 10 000 steps to populate the replay buffer before initiating the learning process. For evaluating sparse Meta-World environments, we provide average success rate evaluations. In this setup, we consider both the average of the final episode success values and the average area under the success rate curve, computed over five seeds.

Statistical Significance. We always highlight the largest IQM in bold in each of the tables. For each of the alternatives we run a one-sided t-test on the null hypothesis that the two models have the same mean. If this null is not rejected at a significance level $p < 0.05$, we also highlight it in bold.

B.4. Hyperparameters and architectures

PBAC specific hyperparameters. PBAC has three hyperparameters: bootstrap rate, a posterior sampling rate, and prior variance. We observe PBAC to work robustly on reasonably chosen defaults. See Appendix D.3 for an ablation on a range of these for the cartpole and delayed ant environments. We list the hyperparameters we used for each environment in Table 5.

Table 5. Hyperparameters specific to PBAC. The chosen bootstrap rate (BR), posterior sampling rate (PSR), prior variance (PV), and Coherence Propagation rate (CPR) for each of the eleven environments.

TASK	BR	PSR	PV
ant	0.05	5	1.0
hopper	0.01	5	1.0
humanoid	0.05	5	1.0
ballincup	0.05	5	1.0
cartpole	0.05	10	1.0
reacher	0.05	5	1.0
ant (delayed)	0.05	5	1.0
ant (very delayed)	0.05	5	5.0
hopper (delayed)	0.05	5	1.0
hopper (very delayed)	0.05	5	1
humanoid (delayed)	0.05	5	1.0
window close (sparse)	0.01	10	5.0
window open (sparse)	0.05	10	1.0
drawer close (sparse)	0.05	10	1.0
drawer open (sparse)	0.05	10	1.0
reach hidden (sparse)	0.01	10	1.0
button press topdown (sparse)	0.05	10	1.0
door open (sparse)	0.05	10	1.0

Table 6. Task description. Description of all tasks for Meta-World sparse environments.

ENVIRONMENT	INSTRUCTION
window-close-v2	Push and close a window.
window-open-v2	Push and open a window.
drawer-close-v2	Push and close a drawer.
drawer-open-v2	Open a drawer.
reach-hidden-v2	Reach a goal position.
button-press-topdown-v2	Press a button from the top.
door-open-v2	Open a door with a revolving joint.

Table 7. Shared hyper-parameters. Hyperparameters used by all methods.

Hyper-parameter	Value
Evaluation episodes	10
Evaluation frequency	Maximum timesteps / 100
Discount factor (γ)	0.99
n -step returns	1 step
Replay ratio	5
number-of-critic-networks	10
Replay buffer size	100,000
Maximum timesteps*	300,000
Number of hidden layers for all networks	2
Number of hidden units per layer	256
Nonlinearity	CReLU
Mini-batch size (n)	256
Network regularization method	Layer Normalization (LN) (Ball et al., 2023)
Actor/critic optimizer	Adam (Kingma & Ba, 2015)
Optimizer learning rates (η_ϕ, η_θ)	3e-4
Polyak averaging parameter (τ)	5e-3

* Ballincup, reacher, and cartpole use a reduced number of maximum steps. The former two use 100,000 and the latter 200,000.

Shared hyperparameters and design choices. We use a *layer normalization* (Ball et al., 2023) after each layer to regularize the network, and a *concatenated ReLU (CReLU)* activation function (Shang et al., 2016) instead of the standard ReLU activation which enhances the model by incorporating both the positive and negative parts of the input and concatenating the results. This activation leads to potentially better feature representations and the ability to learn more complex patterns. Moreover, we rely on a high *replay ratio (RR)* and a small *replay buffer size*, which reduce the agent’s dependence on long-term memory and encourage it to explore different strategies. These are employed to improve the plasticity of the learning process. Recently, Nauman et al. (2024) showed that a combination of these design choices can overall greatly improve the agent learning ability. Additionally, we opted to use the Huber loss function for all baseline models after observing in our preliminary trials that it consistently provided performance advantages across different baselines. The temperature parameter α is automatically adjusted during training to balance exploration and exploitation by regulating policy entropy, following Haarnoja et al. (2018b). All design choices found advantageous for our model and not harmful to other have also been applied to the baselines. Table 7 provides details on the hyper-parameters and network configurations used in our experiments.

Actor and critic networks. Our implementation of PBAC along with proposed baselines share the architectural designs provided in Table 8 for each critic network in the ensemble and actor network. The quantities d_s and d_a denote the dimension of the state space and the action space, respectively. The output of the actor network is passed through a $\tanh(\cdot)$ function for the deterministic actor networks used in BEN and BootDQN-P. We implement the probabilistic actors of DRND and PBAC as a *squashed Gaussian head* uses the first d_a dimensions of its input as the mean and the second d_a as the variance of a normal distribution.

B.4.1. BASELINES

We compare PBAC against a range of state-of-the-art general purpose actor-critic methods that are all empowered by ensembles. All design choices mentioned above found advantageous for our model and not harmful to other have also been applied to the baselines. Below we also explain further changes compared to the original works that we found to be beneficial in preliminary experiments.

BEN. Bayesian Exploration Networks (BEN), introduced by Fellows et al. (2024) serve as the best representative that can learn a Bayesian optimal policy and handle the exploration vs. exploitation tradeoff. We modify BEN by relying on Bayesian deep ensembles (Lakshminarayanan et al., 2017) instead of the normalizing flow-based approach used in the original work. An ensemble of $K - 1$ heteroscedastic critics learns a heteroscedastic univariate normal distribution over the Bellman target, while the K th critic, regularized by the ensemble guides the actor network.

Table 8. Actor and critic architectures. Here, d_s and d_a are the dimensionalities of the state and action spaces.

Actor network	Critic network
Linear (d_s , 256)	Linear ($d_s + d_a$, 256)
Layer-Norm	Layer-Norm
CReLU ()	CReLU ()
Linear (256, 256)	Linear (256, 256)
Layer-Norm	Layer-Norm
CReLU ()	CReLU ()
Linear (256, $2 \times d_a$)	Linear (256, 1)
SquashedGaussian ($2 \times d_a$, d_a)	

Table 9. Hyperparameters specific to BootDQN-P. The chosen bootstrap rate (BR), posterior sampling rate (PSR), and prior scaling (PS) for each of the eleven environments. Changes from the defaults are marked in bold.

TASK	BR	PSR	PS
ant	0.05	5	5.0
hopper	0.05	5	5.0
humanoid	0.1	1	5.0
ballincup	0.05	5	5.0
cartpole	0.05	10	1.0
reacher	0.05	1	1.0
ant (delayed)	0.1	1	1.0
ant (very delayed)	0.05	5	5.0
hopper (delayed)	0.05	5	5.0
hopper (very delayed)	0.05	5	5.0
humanoid (delayed)	0.1	1	9.0
window close (sparse)	0.05	5	5.0
window open (sparse)	0.05	5	5.0
drawer close (sparse)	0.05	5	5.0
drawer open (sparse)	0.05	5	5.0
reach hidden (sparse)	0.05	5	5.0
button press topdown (sparse)	0.05	5	5.0
door open (sparse)	0.05	5	5.0

BootDQN-P. Bootstrapped DQN with randomized prior functions (Osband et al., 2018), a Bayesian model-free approach, serve as a close relative to our method. Throughout all environments we share most parameters with PBAC. Changes for specific parameters are discussed in Table 9, and rely on a Thompson sampling actor. Its randomized priors allow the model to explore even in the presence of sparse reward. A prior scaling (PS) parameter regulates their influence.

DRND. Distributional randomized network distillation (DRND) (Yang et al., 2024), model the distribution of prediction errors from a random network. This distributional information is used as signal to guide exploration. As in the original work, we integrate it into a soft actor-critic (SAC) (Haarnoja et al., 2018a) framework. This random predictor network is trained via the same objective and uses the same architecture as proposed by Yang et al. (2024). Actor and critic networks follow the architectural choices described above. Additionally, we optimize the α scaling parameter in the SAC as is common practice.

C. Pseudocode

For illustrative purposes, we demonstrate the algorithmic steps for a deterministic actor training setting in Algorithm 1. However, in the experiments we use its soft actor version where the policy network follows a squashed Gaussian distribution, Bellman targets are accompanied a policy entropy bonus, and the entropy coefficient is learned following the scheme introduced in Soft-Actor Critic Applications (Haarnoja et al., 2018a). The automatic entropy tuning mechanism dynamically

adjusts the temperature parameter α , balancing exploration and exploitation by controlling entropy’s influence in the objective function.

D. Further results

D.1. Reward curves

See Figure 2 for the full reward curves of all MuJoCo and DMControl environments corresponding to the results presented in Table 1 in the main text. Success rate for Meta-World environments are available in Figure 3, and their corresponding results are available in Table 2

D.2. State space visualizations

Throughout the training, we record the currently visited state at regular intervals and plot them in five groups, for PBAC and each of the baselines. We visualize two environments: cartpole and delayed ant. In each case we record every 500th step over the whole training process and record the corresponding state. The whole set is split into five groups and each is plotted as its own scatter plot.

D.2.1. CARTPOLE

Of cartpole’s five state dimensions, only the first two are interpretable, giving us the position of the cart and the cosine of the angle of the pole. We visualize them in Figure 4. As discussed above, the agent gets rewarded only if it manages to stay close to the zero with an upwards pole, i.e., an angle close to one.

PBAC is able to quickly explore the state space and then concentrate on visiting the states with high reward (red zone), while remaining flexible enough to explore further regions. BEN similarly is able to quickly identify the target region, but starts to fully exploit it and loses its flexibility in the process. As reported in Table 1, they end each episode with a similar performance.

Similar to it, BootDQN-P has no problem in exploring the state space, however it never manages to find the narrow target and thus never converges. BEN starts exploring a wide range of states, but ultimately gets stuck in this seed without being able to find the target. As shown in Figure 2 BEN’s performance varies greatly depending on the random initial seed in this environment. As such, this is a random representative of a failure case, not of its general performance on cartpole. DRND quickly gets stuck as well within a small subset of the state space, essentially just exploring the position of the cart within ever being able to significantly change the angle of the pole.

D.3. Effects of the hyperparameters

We evaluate the sensitivity of the training process of PBAC with respect to its three main hyperparameters, bootstrap rate (BR) κ , posterior sampling rate (PSR), and prior variance (PV) σ_0 of ρ_0 , on two environments, cartpole and delayed ant. Depending on the environment, PBAC is sensitive to their choice (see Figure 5 on the cartpole environment), and shows clearly interpretable patterns, or it remains insensitive to their choice as in the delayed ant environment visualized in Figure 6.

Algorithm 1 PAC-Bayesian Actor Critic (PBAC)

- 1: **Input:** Polyak parameter $\tau \in (0, 1)$, mini-batch size $n \in \mathbb{N}$, bootstrap rate κ , posterior sampling rate PSR, prior variance σ_0^2 , number of ensemble elements K
- 2: **Initialize:** replay buffer $\mathcal{D} \leftarrow \emptyset$, critic parameters $\{\theta_k\}$ and targets $\bar{\theta}_k \leftarrow \theta_k$, actor network trunk g and heads h_1, \dots, h_K .
- 3: $s \leftarrow \text{env.reset}()$ and $e \leftarrow 0$ (interaction counter)
- 4: **while training do**
- 5: **if** $\text{mod}(e, \text{PSR}) = 0$ **then**
- 6: $j \sim \text{Uniform}(K)$
- 7: $\pi \leftarrow \pi_{g \circ h_j}(s)$ (Update active critic)
- 8: **end if**
- 9: $a \leftarrow \pi_j(s)$ and $(r, s') \leftarrow \text{env.step}(a)$ and $e \leftarrow e + 1$
- 10: Store new observation: $\mathcal{D} \leftarrow \mathcal{D} \cup (s, a, r, s')$
- 11: Sample minibatch: $B \sim \mathcal{D}$ with $|B| = n$
- 12: Sample a bootstrap mask: $b_{ik} \sim \text{Bernoulli}(1 - \kappa)$, $\forall [n] \times [K]$
- 13: Compute prior mean and posterior moments: $\forall (s_i, a_i, r_i, s'_i) \in B$ do

$$\bar{\mu}_{\pi_{g \circ h_j}}(s'_i) \leftarrow \frac{1}{K} \sum_{k=1}^K b_{ik}(\bar{X}_k(s'_i, \pi_{g \circ h_j}(s'_i)))$$

$$\mu_{\pi_{g \circ h_j}}(s_i) \leftarrow \frac{1}{K} \sum_{k=1}^K b_{ik}(X_k(s_i, \pi_{g \circ h_j}(s_i)))$$

$$\sigma_{\pi_{g \circ h_j}}^2(s_i) \leftarrow \frac{1}{K-1} \sum_{k=1}^K b_{ik}(X_k(s_i, \pi_{g \circ h_j}(s_i)) - \mu_{\pi_{g \circ h_j}}(s_i))^2$$

- 14: Update critics $k \in [K]$:

$$\theta_k \leftarrow \arg \min_{\theta_k} \left\{ \frac{1}{nK} \sum_{i=1}^n \sum_{k=1}^K b_{ik} \left(r_i + \gamma \bar{X}_k(s'_i, \pi_{g \circ h_j}(s'_i)) - X_k(s_i, \pi_{g \circ h_j}(s_i)) \right)^2 \right. \\ \left. + \frac{1}{nK} \sum_{i=1}^n \sum_{k=1}^K \frac{b_{ik} \left(r_i + \gamma \bar{\mu}_{\pi_{g \circ h_j}}(s'_i) - X_k(s_i, \pi_{g \circ h_j}(s_i)) \right)^2}{2\gamma^2 \sigma_0^2} - \frac{\gamma^2 + 1/2}{n} \sum_{i=1}^n \log \sigma_{\pi_{g \circ h_j}}^2(s_i) \right\}$$

- 15: Update actor:

$$(g, h_1, \dots, h_K) \leftarrow \arg \max_{g, h_1, \dots, h_K} \left[\frac{1}{nK} \sum_{i=1}^n \sum_{k=1}^K X_k(s_i, \pi_{g \circ h_k}(s_i)) \right]$$

- 16: Update critic targets: $\bar{\theta}_k \leftarrow \tau \theta_k + (1 - \tau) \bar{\theta}_k$ for $k \in [K]$
- 17: **if** episode end **then** $s \leftarrow \text{env.reset}()$ **else** $s \leftarrow s'$
- 18: **end while**

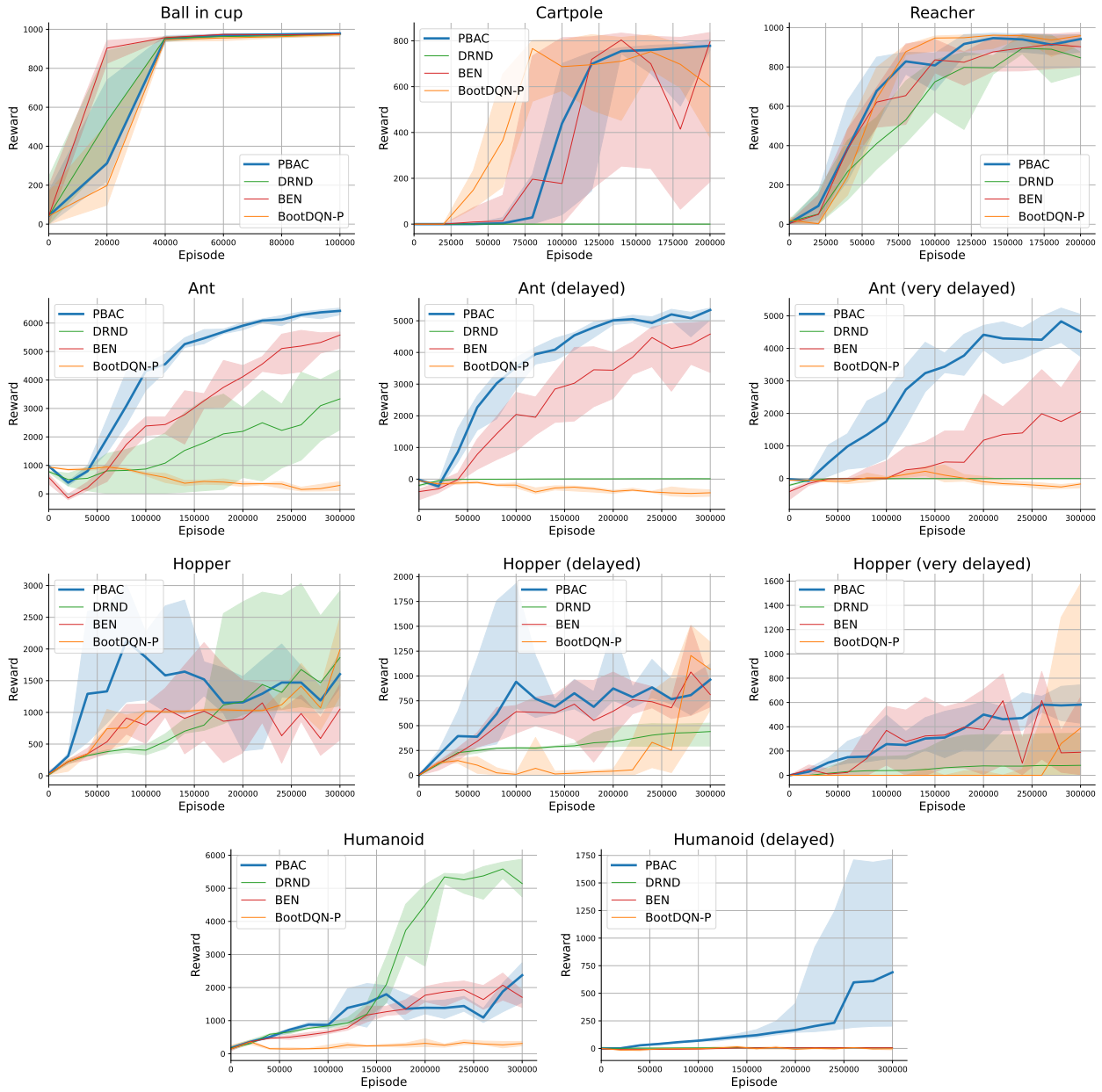


Figure 2. Reward curves. The reward curves for all environments throughout training corresponding to the results presented in Table 1. Visualized are the interquartile mean together with the interquartile range over ten seeds.

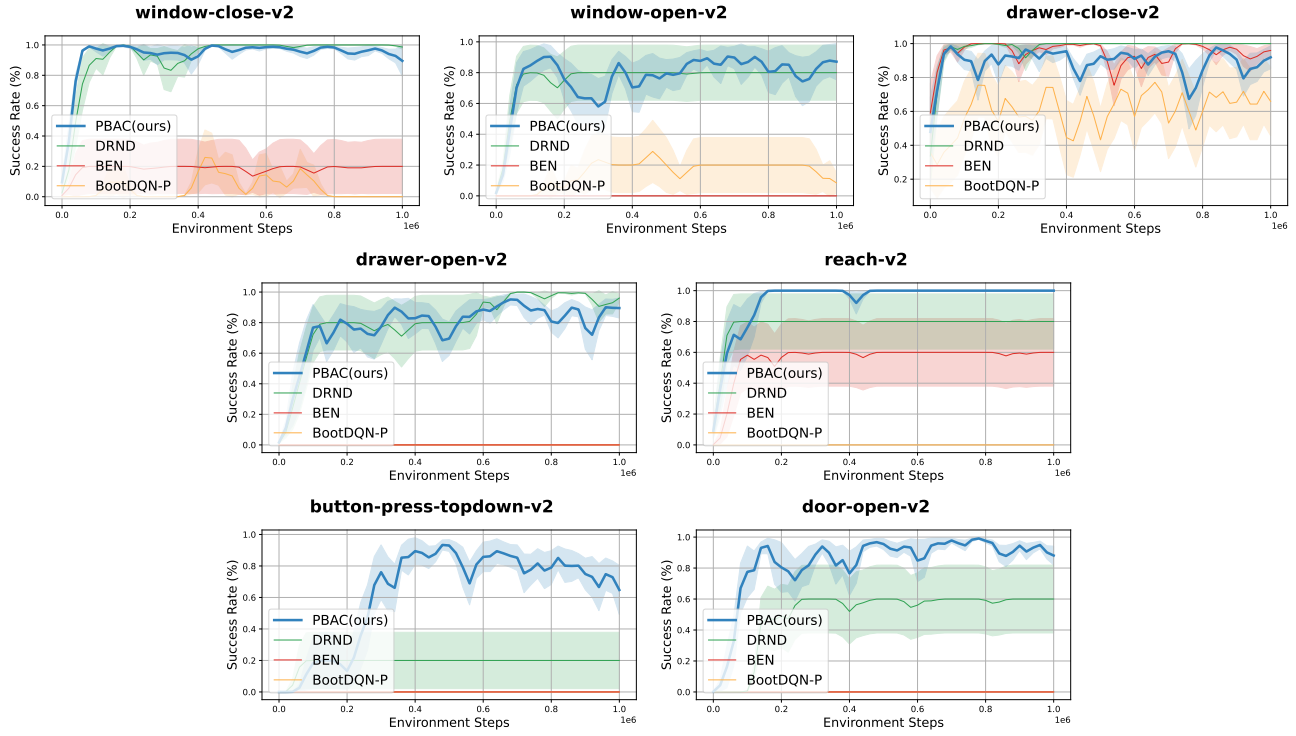


Figure 3. Success rate curves. The success rate curves for sparse Meta-World environments throughout training corresponding to the results presented in Table 2. Visualized are the mean over five seeds.

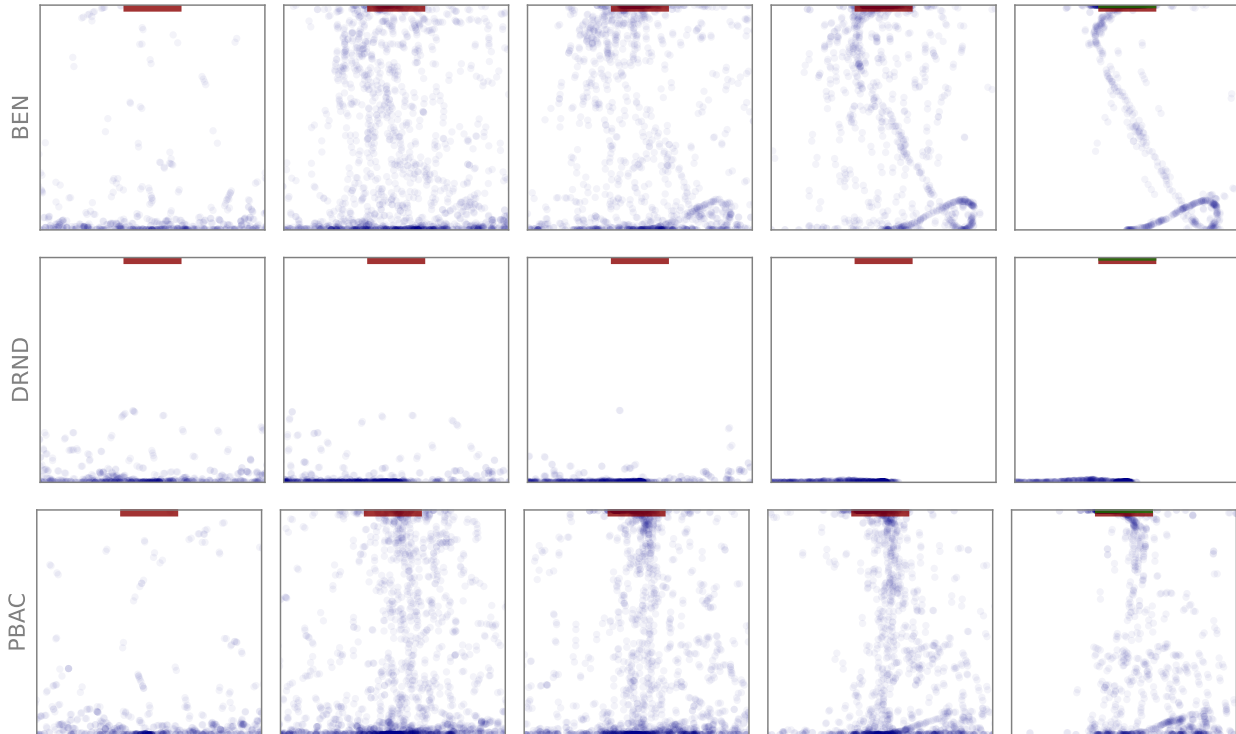


Figure 4. State visitation frequency for cartpole. The visualization shows seed 1.

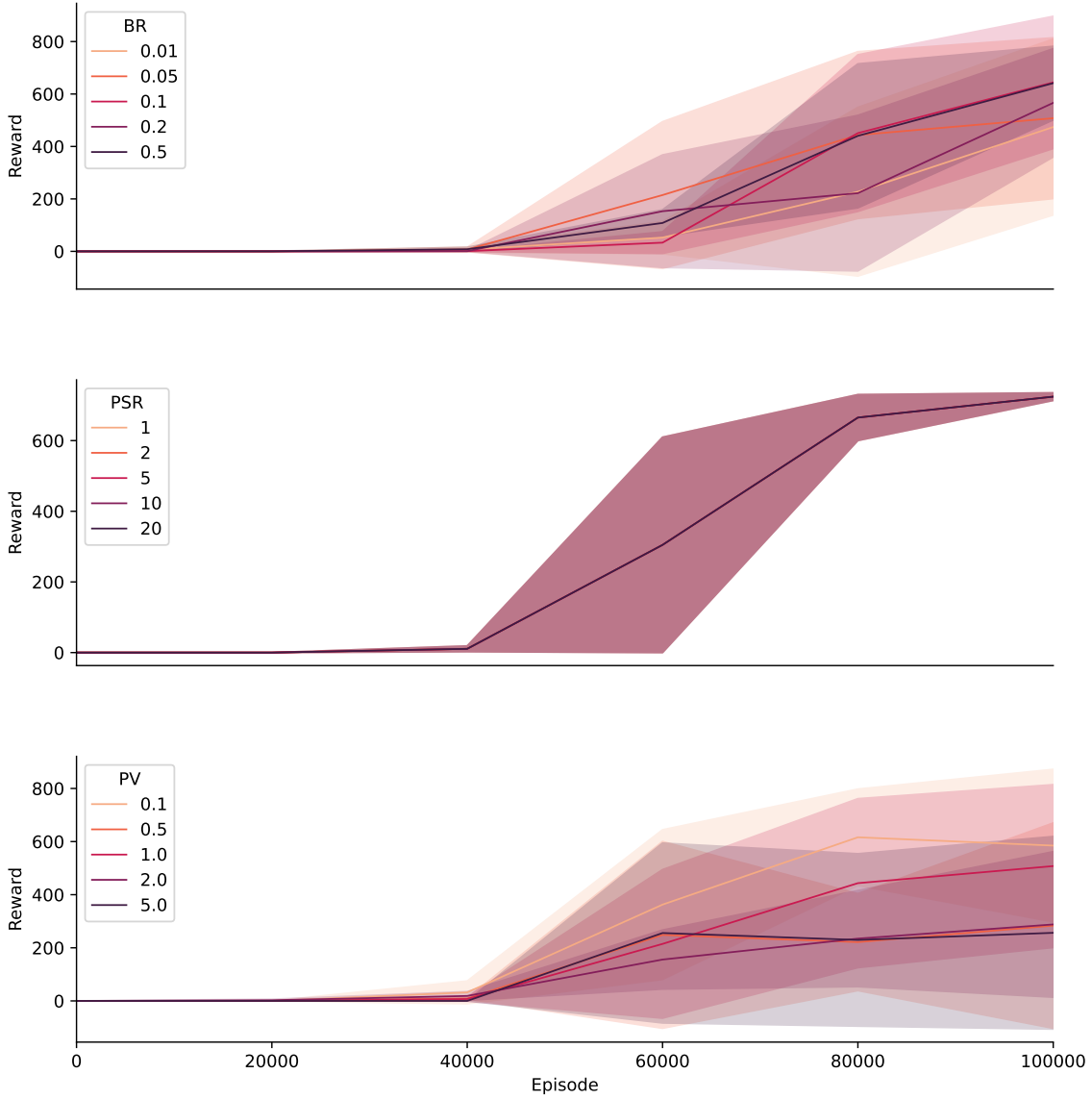


Figure 5. Ablation results on cartpole. We show varying bootstrap rates (BR), posterior sampling rates (PSR), and prior variances (PV). While PBAC is mostly robust in terms of varying prior variances, increases in the bootstrap rate and decreases in the posterior sampling rate delay the learning process. Visualized are the interquartile mean together with the interquartile range over three seeds.

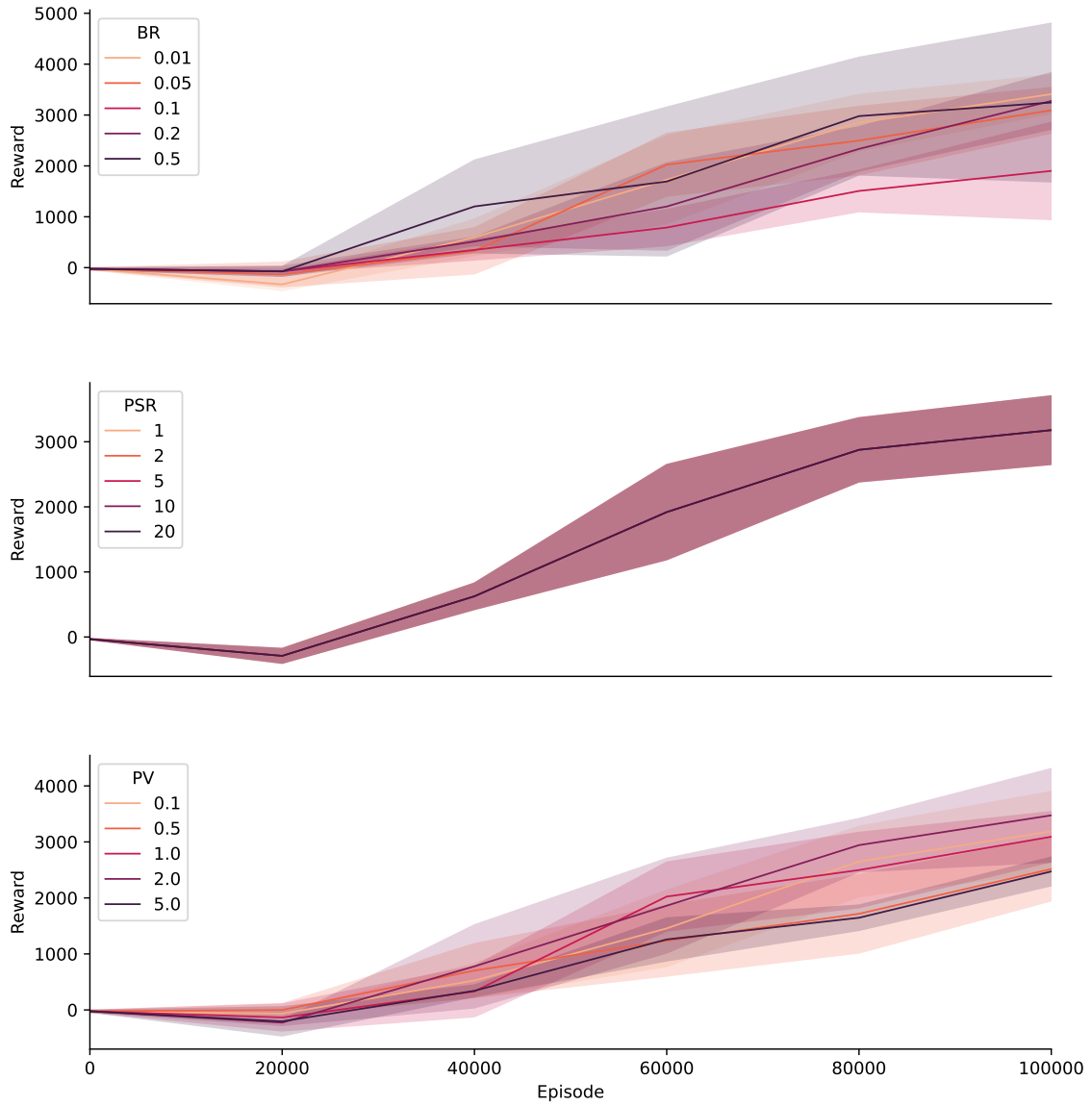


Figure 6. Ablation results on delayed ant. We show varying bootstrap rates (BR), posterior sampling rates (PSR), and prior variances (PV). Compared to the ablation on cartpole (see Figure 5), PBAC is robust against variations in all three hyperparameters in the delayed ant environment. Visualized are the interquartile mean together with the interquartile range over three seeds.